NASA TECHNICAL NOTE

NASA TN D-4750



# DESCRIPTIONS AND OPERATING PARAMETERS OF A MACH 2 NOZZLE SYSTEM FOR THE LANGLEY 11-INCH CERAMIC-HEATED TUNNEL

*by Kenneth Sutton*

*Langley Research Center*
*Langley Station, Hampton, Va.*

NATIONAL AERONAUTICS AND SPACE ADMINISTRATION • WASHINGTON, D. C. • SEPTEMBER 1968

NASA TN D-4750

# DESCRIPTION AND OPERATING PARAMETERS OF A MACH 2 NOZZLE SYSTEM FOR THE LANGLEY 11-INCH CERAMIC-HEATED TUNNEL

By Kenneth Sutton

Langley Research Center
Langley Station, Hampton, Va.

NATIONAL AERONAUTICS AND SPACE ADMINISTRATION

For sale by the Clearinghouse for Federal Scientific and Technical Information
Springfield, Virginia 22151 – CFSTI price $3.00

# DESCRIPTION AND OPERATING PARAMETERS OF A MACH 2 NOZZLE SYSTEM FOR THE LANGLEY 11-INCH CERAMIC-HEATED TUNNEL

By Kenneth Sutton
Langley Research Center

## SUMMARY

A Mach 2 nozzle system has been developed to operate interchangeably with existing Mach 4 and Mach 6 systems previously available for high-temperature materials research at the Langley 11-inch ceramic-heated tunnel. An experimental evaluation, using air as the test gas, was made to determine the operating parameters of this system and to define the test environment. Of particular concern were the definition of stream total temperature decay with time and the damage to test specimens due to stream contamination. The diameters of the calibration models and probes were approximately three-fourths of the diameter of the nozzle exit.

The experimental results showed that the Mach 2 system has a linear decrease of total temperature of approximately $200^{\circ}$ R ($110^{\circ}$ K) in a test time of 600 seconds for the standard operating range of chamber pressure of 115 to 165 psia (0.79 to 1.14 $MN/m^2$). The total temperature range as measured was $2100^{\circ}$ R to $4000^{\circ}$ R ($1170^{\circ}$ K to $2220^{\circ}$ K). The damage to a test model due to stream contamination from the ceramic bed, as measured by effects on graphite models, is such that it can be neglected for a significant number of experimental material programs. Also, the comparison in pressure, heating-rate, and shear distributions indicates the suitability of material response tests at the stagnation region of a model.

The results in this report can be used to determine the applicability of the Mach 2 system of the Langley 11-inch ceramic-heated tunnel for an experimental program and to select the desired operating parameters.

## INTRODUCTION

The continual advancement in reentry materials research makes it necessary to construct new ground test facilities and to improve existing facilities. In order to extend the capabilities of the Langley 11-inch ceramic-heated tunnel, a Mach 2 system has been developed to fit interchangeably with the existing Mach 4 and Mach 6 systems. (See ref. 1.)

The Mach 4 system, as presently installed, operates at high air pressures and high mass-flow rates. The heat storage of the facility is not sufficient at these high mass-flow rates to operate for long test times without a large decrease in total temperature of the airstream. Furthermore, the high pressures and mass-flow rates can lift dust particles from the heat-exchanger bed and cause serious contamination of the airstream. It is possible for this contamination to cause erosion of the material of the test specimens and thus make this type of facility unsuitable for studies of oxidation or ablation processes on thermal protection materials.

The primary purpose of the installation of the Mach 2 system in the Langley 11-inch ceramic-heated tunnel was to obtain long test times with a small decrease in total temperature of the stream and low contamination of the stream at model pressures and heating rates comparable to those obtained in the Mach 4 nozzle. The throat size would not have to be any larger than the present Mach 4 system in order to accommodate a model of sufficient size for test purposes. Because of the lower operating pressures and mass flows, there should be a reduction in the dust contamination of the stream. Since the heat-storage capacity of the tunnel would remain the same, the total temperature of the stream should not decrease as rapidly and a more uniform temperature should prevail during a test.

In the present study a Mach 2 system, utilizing three contour nozzles with different size throats, was installed in the Langley 11-inch ceramic-heated tunnel and an evaluation was made of its operating parameters. Measurements were made of the total temperature, total pressure, and heating rate of the airstream. The stream contamination was not measured directly but its effect was evaluated by comparison of the damage done to graphite models. Also, some measurements were made of the pressure and heating-rate distributions around test models.

This report presents a description of the Mach 2 system as installed in the Langley 11-inch ceramic-heated tunnel and gives the flow properties as measured and calculated in the study.

## SYMBOLS

The units used for the physical quantities defined in this paper are given both in the U.S. Customary Units and in the International System of Units (SI). (See ref. 2.) Appendix A presents a table of conversion factors between these two systems of units.

$c$ calorimeter material specific heat, British thermal units/pound mass-$^{o}$Rankine (joules/kilogram-$^{o}$Kelvin)

| | |
|---|---|
| $H$ | enthalpy, British thermal units/pound mass (joules/kilogram) |
| $N_{Re}$ | Reynolds number per unit length, $feet^{-1}$ ($meters^{-1}$) |
| $p$ | pressure, pounds/square inch absolute (meganewtons/$meter^2$) |
| $\dot{q}$ | cold-wall heating rate, British thermal units/$foot^2$-second (watts/$meter^2$) |
| $R$ | cylindrical radius of models (see figs. 9 and 10), inches (meters) |
| $R_{eff}$ | effective nose radius, inches (centimeters) |
| $s$ | distance from stagnation point along surface, inches (meters) |
| $T$ | temperature, $^{o}$Rankine ($^{o}$Kelvin) |
| $t$ | time, seconds |
| $V$ | velocity, feet/second (meters/second) |
| $x$ | calorimeter thickness, feet (meters) |
| $\rho$ | density, pounds mass/$foot^3$ (kilograms/$meter^3$) |
| $\tau$ | aerodynamic shear, pounds force/$foot^2$ (kilonewtons/$meter^2$) |
| $\phi$ | radial angle station (see fig. 9), degrees |

Subscripts:

| | |
|---|---|
| $c$ | settling chamber |
| $l$ | local condition |
| $s$ | stagnation point |
| $t$ | total condition |
| 1 | condition upstream of normal shock |

| | |
|---|---|
| 2 | condition downstream of normal shock |
| w | thermocouple wire |
| e | equilibrium |

## FACILITY

A complete description of the Langley 11-inch ceramic-heated tunnel and the Mach 4 and Mach 6 systems is given in references 1 and 3. This tunnel uses a heat exchanger of ceramic pebbles to transfer heat to the test gas before the gas expands through a nozzle system.

### Heat Exchanger

A diagram of the heat exchanger of the Langley 11-inch ceramic-heated tunnel is shown in figure 1. This unit consists of a 54-inch (1.35-meter) diameter pressure vessel approximately 30 feet (9.15 meters) high which is lined with ceramic bricks and filled with 20 feet (6.11 meters) of 3/8-inch (0.95-cm) ceramic pebbles. The pebble bed is heated by the downward flow of combustion gases from a burner located at the top of the heat exchanger. The burner is turned off after the pebbles have been heated to the desired temperature and the test gas enters the bottom of the pressure vessel and is heated by passing through the pebbles. The heated test gas then flows through a nozzle system connected to the top of the heat exchanger. The top of the pebble bed can be heated to a maximum temperature of $4560^{\circ}$ R ($2530^{\circ}$ K) which is the maximum temperature usage of the zirconia pebbles and bricks located at the top of the heat exchanger. (See refs. 1 and 4.)

### Mach 2 Nozzles

Three water-cooled axisymmetric contour nozzles with nominal throat diameters of 1/2, 3/4, and 1 inch (1.3, 1.9, and 2.5 cm) were designed for use with the heat exchanger and evaluated in the present study. A photograph showing the arrangement of a Mach 2 nozzle as connected to the heat exchanger is shown in figure 2. As shown in the photograph, the Mach 2 system is a free-jet system and is interchangeable with the Mach 4 and Mach 6 systems by the use of a water-cooled adapter plate.

The normal operating range of chamber pressure for the Mach 2 system is 115 to 165 psia (0.79 to 1.14 $MN/m^2$); however, it may be operated to pressures as high as 350 psia (2.42 $MN/m^2$).

The nozzles of the Mach 2 system are identified by their nominal throat diameters. A section view of the 1-inch (2.5-cm) nozzle is shown in figure 3. The 1/2- and 3/4-inch (1.3- and 1.9-cm) nozzles are similar in construction. The coordinates of the nozzles downstream of the throat are given in table I.

The test gas for the Mach 2 system can be varying mixtures of air and nitrogen. A calibrated orifice arrangement is used to control and measure the flow rates of air and nitrogen which is then mixed and piped to the bottom of the heat exchanger. The test gas mixture can be varied from full air to full nitrogen with almost continuous mixtures in between.

## MEASUREMENT TECHNIQUES AND CALIBRATION MODELS

### Test Procedure

The test procedure was basically the same for all the tests. The pebble bed was heated to the proper temperature by the standard facility procedure. The vessel was then pressurized to the correct chamber pressure. A piston mechanism inserted the calibration model into the test stream for the specified exposure time. Air was used as the test gas for all tests.

The two parameters which are used to set the test stream conditions are "fire-on" temperature of the pebble bed and chamber pressure. "Fire-on" temperature is the temperature of the top of the bed with the burner fire on. This temperature is measured with an optical pyrometer through the quartz sight glass at the top of the heat exchanger. (See fig. 1.) A Bourdon-tube dial gage is connected to a pressure tap in the settling chamber (see fig. 1) and is used to measure chamber pressure. The test gas flow is adjusted to maintain the specified chamber pressure. The gas velocity in the settling chamber is so low that the measured pressure can be considered as total pressure.

The voltage outputs from all model thermocouples were recorded on an oscillograph recorder. All pressures from test models were measured with electrical strain-gage transducers and recorded on an oscillograph recorder. A description of the test models and any special procedures are given in the following sections.

### Stream-Contamination Measurements

There was no direct measurement of stream contamination; however, the effect of contamination was measured by the damage to graphite models. These tests were made with a cold bed (pebble bed at ambient temperature) to avoid oxidation of the graphite by a heated airstream. Tests were made in each of the Mach 2 nozzles at a chamber pressure of 115 psia (0.79 $MN/m^2$) and exposure times of 30 and 240 seconds. Also, tests were made before and after cleaning of the pebble bed.

The models were hemisphere-cylinders with a 0.250-inch (0.635-cm) radius and had a removable center plug. Details of the model are shown in figure 4. The complete model and the center plug were weighed on an analytical balance before and after a test. Weight loss and appearance of the model after testing was the basis for evaluation of model damage due to test-stream contamination.

## Total Temperature Measurements

The total temperature of the jet airstream was measured by the use of seven different designs of thermocouple probes which are described in figure 5. The probes were different in regard to type of thermocouple, outer and inner shield construction, and overall size. Two types of thermocouple wires were used:

(1) Platinum—platinum—13-percent rhodium

(2) Iridium—iridium—40-percent rhodium

A typical probe mounted in a support sting is shown in figure 6.

A discussion of thermocouple probe design used for gas stream measurements and their errors is contained in reference 5. In the present study the thermocouple probes were designed so that only the radiation error had to be applied to the measured temperature. The conduction error was made sufficiently small by the proper sizing of the length-diameter ratio of the thermocouple wire. The vent holes in the stagnation cups that allow an air flow to pass the thermocouple bead were sized so that the velocity error was negligible. The radiation error was computed by the method outlined in appendix B. The various thermocouple designs were used in order to have an evaluation of the radiation error and to select a design for randomly checking the total temperature during general operation of the Mach 2 system.

Only one thermocouple design was used during a particular test. The thermocouple probe was inserted in the airstream for approximately 2 seconds and this insertion was repeated every 60 seconds for the duration of the test. This procedure allowed for a measurement of the temperature decay with time. The probes could not be left in the stream continuously because the stagnation cups would have melted. The initial insertion of the thermocouple was taken as time zero and was from 180 to 240 seconds from the time the burner was cut off.

The 1-inch (2.5-cm) nozzle was used in the measurement of total temperature at chamber pressures of 115 and 165 psia (0.79 and 1.14 $MN/m^2$). The pebble bed was heated to nominal fire-on settings of 2460°, 2960°, 3460°, 3960°, and 4460° R (1370°, 1650°, 1920°, 2200°, and 2480° K). All measurements were taken along the center line of the nozzle at a distance of 0.25 or 0.50 inch (0.64 or 1.27 cm) from the nozzle exit.

## Pressure Measurements

The total pressure behind the shock wave was measured with three total-pressure probes. (See fig. 7.) The probes were hemisphere-cylinders with diameters of 0.375, 0.500, and 1.000 inch (0.953, 1.270, and 2.540 cm). The probes were mounted in a 1-inch (2.54-cm) diameter water-cooled support sting as shown in figure 8.

Several measurements of total pressure behind the shock wave were made during a test. The chamber pressure would be set and the probe inserted in the airstream for approximately 5 seconds; then another chamber pressure would be set and a new measurement was made. This process was repeated as required for each test. Measurements of impact pressure were made in each of the three nozzles at several longitudinal locations downstream from the exit plane of the nozzles along the center line of the jet airstream.

Measurements of the pressure distribution around a hemispherical nose and a blunt-nose model were made in the 1-inch (2.5-cm) nozzle at several airstream conditions. Sketches of the exterior shape of the pressure distribution models and their orifice locations are shown in figure 9. The inside diameter of the pressure orifice was 0.020 inch (0.051 cm).

## Heating-Rate Measurements

Measurements of the cold-wall stagnation-point heating rate of three nose shapes and the heating-rate distribution around a hemisphere cylinder were made in the 1-inch (2.5-cm) nozzle. Both thin-wall slope-type calorimeters and continuous reading calorimeters were used for the measurements. The stagnation-point heating rate was measured over a range of test conditions whereas the heating-rate distribution around the hemisphere cylinder was measured at only two conditions.

A sketch of the thin-wall slope-type calorimeters is shown in figure 10. Model 1 had a wall thickness of 0.025 inch (0.064 cm) with a thermocouple on the inner wall at only the stagnation-point location. This calorimeter was used for the measurement of stagnation-point heating rate to a hemisphere at the milder test conditions. Model 2 had a wall thickness of 0.074 inch (0.188 cm) with six thermocouple locations. This calorimeter was used for the heating-rate distribution measurements and the test conditions were more severe than those for model 1. Both calorimeters were made from type 347 stainless steel and had 30-gage chromel-alumel thermocouples.

The experimental heating rate for the thin-wall slope-type calorimeters were calculated by the use of the temperature rise with time at the inner wall and the physical properties of the calorimeter material. The heating rate for the calorimeter with the thinner wall (model 1) was calculated by the usual equation for slope-type thin-wall calorimeters:

$$\dot{q} = \rho x c \frac{dT}{dt}$$

The heating rates for model 2, because of its thicker wall, were calculated on an electronic digital computer with a finite block solution of the heat balance on each block. A two-dimensional heat-conduction method was used for an axisymmetrical body and the entire shell of the model was broken into small blocks and used in the solution. The heating rates around the exterior body were the main inputs for the program on a trial-and-error basis. The correct solution was assumed when the temperature at the inner wall matched the experimental data.

Continuous reading calorimeters of two body shapes were also used in the measurement of stagnation-point heating rates. These instruments were commercially made and sketches of their exterior shapes are shown in figure 11. The continuous reading calorimeter has a thin-foil constantan sensing element attached to a copper body acting as a heat sink (in this case, a water-cooled heat sink). One side of a thermocouple is connected to the center of the sensing element and the other side is attached to the heat sink. The voltage output from the thermocouple is directly proportional to the cold-wall heating rate to the sensing element. The analysis for this type of calorimeter is given in reference 6. The calibration curves relating cold-wall heating rate to voltage output were supplied by the manufacturer.

## RESULTS AND DISCUSSION

### Test-Stream Contamination

In a ceramic-heated facility the test stream can become contaminated as the test gas flows through the ceramic bed by the pick up of dust from the pebbles and brick liner. This contamination may cause damage to a test specimen by eroding and/or pitting the surface of the specimen. In the present study the degree of test-stream contamination was evaluated on the basis of apparent damage and weight loss to a graphite model in a cold stream.

The results of the measurements, in terms of weight loss from the models, are given in table II. The appearances of the models after testing are shown in the photographs in figure 12. The apparent damage to the graphite models decreased with a decrease in the size of the nozzle throat. An increase in damage was evident with an increased time of exposure to the airstream. However, an examination of table II shows that the graphite mass loss did not increase proportionally with time. Hence, the possible damage to a test specimen can be reduced by allowing a time period (approximately 60 seconds) to elapse between reaching test-stream equilibrium conditions and before insertion of the test specimen. As a basis for comparison, the amount of graphite which

would be removed from the center plug by oxidation in a 240-second test at a stream temperature of 4000° R (2220° K) has been calculated to be 0.0700 gram as compared with 0.0021 gram because of contamination for the 1-inch (2.5-cm) nozzle. Thus, even for the 1-inch (2.5-cm) nozzle and for the longer test times, the contamination should not affect the results of most experimental studies including material studies.

The apparent damage to a graphite model in the Mach 2 system is compared in figure 13 with the damage for a model tested in the Mach 4 system for normal operating chamber pressures in each nozzle. The photograph illustrates the greater damage in the Mach 4 system and that the pits in the model surface are larger for the Mach 4 nozzle than for the Mach 2 nozzle. The model pressures $p_{t,2}$ for the two nozzles are of the same order of magnitude but the mass-flow rate through the Mach 4 nozzle is ten times greater than that through the Mach 2 nozzle.

It is necessary to clean and repair the ceramic bed of the heat exchanger periodically because continued operation of the tunnel damages the zirconia brick liner and the zirconia pebbles. The effect of cleaning and repairing the ceramic bed on the model damage is shown by the photograph in figure 14. As can be seen by the photograph, the damage to a graphite model is greater before the cleaning of the bed than after the cleaning. The facility has to be shut down for approximately 3 to 6 weeks during the cleaning and repairing of the heat exchanger. The previously discussed measurements of model damage were made immediately before cleaning the bed and represent the worst damage to a model.

## Total Temperature of Airstream

The results of the total temperature measurements are given in tables III and IV and are shown in figures 15 to 16. The total temperature decay with time was linear and test times up to 660 seconds can be obtained with a temperature decrease of 10 percent. There was no significant effect of chamber pressure on the total temperature decay between the range of 115 to 165 psia (0.79 to 1.14 MN/m$^2$) as shown in figure 16. Also, there is no significant effect of bed condition (clean or dirty) on the total temperature, and the temperature is repeatable over a long period of time.

The temperature measurements for the various thermocouple designs were in good agreement. The average variation was ±100° R (55° K) for a particular fire-on setting. The maximum radiation correction applied to any thermocouple in this test series was 3.5 percent. Since only one thermocouple was used during a particular test, the variation of ±100° R (55° K) also indicates good repeatability of the tunnel.

A correlation between the total temperature of the airstream and the temperature characteristics of the pebble bed is of particular interest in the operation of a ceramic-heated tunnel. In table III various surface temperatures at the top of the pebble bed are

listed for each test. As previously stated, fire-on temperature is the surface temperature of the bed with the burner on. The "fire-off" temperature is the surface temperature with the burner off and before the test gas is flowing through the bed. The "after-run" temperature is the surface temperature after a test is completed. The average of the fire-off and after-run temperatures is known as the "average-bed" temperature. These temperatures are measured through the quartz sight glass with an optical pyrometer. The average total temperature of the airstream (averages of approximately 360 seconds) is approximately a linear function of all the surface temperatures for the conditions tested. The average-bed correlation with total airstream temperature is shown as a typical example in figure 17.

Although most of the temperature measurements were made only up to 360 seconds, the total temperature decay with time of the Mach 2 system is sufficiently low to allow the system to be used for test times up to 660 seconds. Average curves of the total temperature history in the 1-inch (2.5-cm) nozzle are shown in figure 18. By knowing the fire-on temperature and using figure 18, the total temperature of the test stream can be determined for the chamber pressure range of 115 to 165 psia (0.79 to 1.14 $MN/m^2$). Although no temperature measurements were made in the smaller nozzles, these same curves should be good although the temperature decrease might be slightly less because of lower mass flows. The average total temperature for each fire-on setting should be of sufficient accuracy to use for higher pressure short-time tests. Since the various thermocouple probes were in good agreement, a probe simple in construction, such as designs 2 and 7 (see fig. 5), would be sufficient to spot check the total temperature.

## Total-Pressure Measurements

The results of the total-pressure measurements are given in table V. The measured total-pressure ratio across the shock wave and the normal-shock tables and caloric-imperfection curves of reference 7 were used to determine the Mach number.

The measured relationship between the total pressure behind the shock wave $p_{t,2}$ and the chamber pressure $p_c$ for each of the three nozzles is shown in figures 19, 20, and 21. It should be noted that the chamber pressure $p_c$ is the same as the total pressure of the jet free stream $p_{t,1}$ in the absence of any shock-wave or expansion-wave disturbance. These measurements are for an axial distance from the exit plane of the nozzle of 0.50 inch (1.27 cm) for the 1-inch (2.5-cm) and 3/4-inch (1.9-cm) nozzles and 0.12 inch (0.32 cm) for the 1/2-inch (1.3-cm) nozzle. The pressure ratio across the shock wave and corresponding Mach number are given in the figures for the respective nozzles.

The variation of the total pressure behind the normal-shock wave with axial distance from the nozzle exit is shown in figure 22 for the 1-inch (2.5-cm) nozzle at nominal

chamber pressures of 115 and 165 psia (0.79 and 1.14 MN/m$^2$). Also shown is the Mach number associated with the pressure ratio. At a location between 1.0 and 1.5 inches (2.54 and 3.81 cm) from the nozzle exit, a disturbance occurs and this disturbance, as expected, is the apex of the first flow diamond caused by the expansion waves from the underexpanded flow for the 165 psia (1.14 MN/m$^2$) chamber pressure and by the shock wave from the overexpanded flow for the 115 psi (0.79 MN/m$^2$) pressure. The Mach numbers shown in figure 22 and listed in table V for the data points after the disturbance are not true Mach numbers since chamber pressure is used for $p_{t,1}$ and are only given for the purpose of illustrating the disturbance. A shadowgraph of the airstream (fig. 23(a)) shows the location of the apex of the shock diamond to be approximately 1.2 inches (3.0 cm) from the nozzle exit for a chamber pressure of 115 psia (0.79 MN/m$^2$).

Also shown in figure 23 is a pluming of the test stream and interaction of the flow diamond shock wave with the bow shock of the model which occurs when large models are inserted in the stream. Small-diameter models, such as those with diameters of 3/8 and 1/2 inch (0.95 and 1.27 cm), do not cause any significant pluming of the stream. As shown in figure 23(c), large-diameter models, such as those with diameters of 3/4 and 1 inch (1.90 and 2.54 cm), will cause a significant pluming of the stream. Good reproducible shadowgraphs for 1-inch (2.54-cm) diameter models were not available for this report; however, the degree of pluming is the same as that for the 3/4-inch (1.90-cm) models.

Because of the formation of the flow diamond, models should be tested in the region up to 1.0 inch (2.5 cm) from the nozzle exit for the 1-inch (2.5-cm) nozzle. From similar results for the other two nozzles, models should be tested in the region up to 0.7 inch (1.8 cm) for the 3/4-inch (1.9-cm) nozzle and 0.4 inch (1.0 cm) for the 1/2-inch (1.3-cm) nozzle.

The Mach number in the Mach 2 system is a weak function of total temperature because of calorific imperfections. Measurements in the 1-inch (2.5-cm) nozzle (tests 1 to 4) at total temperatures from 2300$^\circ$ R to 4000$^\circ$ R (1330$^\circ$ K to 2220$^\circ$ K) did not indicate any significant variation in exit Mach number as shown in table V and verified in reference 7.

## Stagnation-Point Heating-Rate Measurements

The cold-wall stagnation-point heating rates to models with three nose shapes as illustrated in figures 10 and 11 were measured in the 1-inch (2.5-cm) nozzle over a range of test conditions. The test conditions and results are given in table VI. The theoretical value of heating rate to the stagnation point was calculated for each test condition and body shape by the theory of reference 8 and is also listed in table VI. The

effective nose radii (equivalent hemispherical radius) used in the theoretical calculations for the flat-face and blunt-nose calorimeters were taken from reference 9 and are listed in table VI.

The comparison between the measured and theoretical heating rates to the stagnation point is shown in figure 24. For perfect agreement the measured values would have to lie on the straight line. There were fluctuations in the read-out traces of the continuous-reading calorimeters and the maximum and minimum values are represented by the limits of the bars in figure 24. The data point is the average heating rate during the exposure time. The maximum and minimum values are listed in table VI as well as the average values. The cause of the fluctuations for the continuous reading calorimeter is not known. Neither the pressure measurements nor the total temperature measurements indicated any type of fluctuation in the airstreams. Also, the large volume in the heat exchanger above the pebble bed should be sufficient to settle out any disturbance in the airstream prior to expansion through the nozzle. The continuous reading calorimeters are extremely sensitive and have shown similar fluctuations in other facilities.

When only the average values for the continuous reading calorimeters were considered, the measured stagnation-point heating rates agreed with the theory to within ±20 percent. The theory of reference 8 and use of the effective nose radii from reference 9 seem to be adequate to calculate the stagnation-point heating rate to a model in the Mach 2 system.

### Model-Pressure, Heating-Rate, and Shear Distributions

The pressure distribution around the exterior of a hemisphere-nose cylindrical-body model and a blunt-nose cylindrical-body model was measured at two test conditions for each model shape in the 1-inch (2.5-cm) nozzle. Heating-rate and aerodynamic-shear distributions for laminar flow were calculated from the pressure distribution data by the use of an electronic digital computer program based on the theory of reference 10.

The distributions for the hemispherical model are shown in figures 25, 26, and 27. The present measured pressure distributions (fig. 25) are compared with the measured data for a sphere from reference 11 and with modified Newtonian theory. Away from the stagnation region ($S/R > 0.6$), the present data is much lower than the other results and indicate a greater expansion; this effect may be due to the pluming of the stream (as previously discussed) because of the large model. The heating-rate and shear distributions calculated from the present measured pressure data are shown in figures 26 and 27, respectively, and are compared with calculations for the modified Newtonian pressure distribution. Also, the measured heating-rate data are compared with the calculated results in figure 26.

The distributions for the blunt-nose model are shown in figures 28, 29, and 30. The measured pressure distribution for this shape was in good agreement with the data of reference 12 which had a similar nose shape.

The heating rate at the stagnation point depends upon the square root of the velocity gradient at the stagnation point. For the hemispherical model the square root of the velocity gradient at the stagnation point for the measured data was slightly higher but within 6 percent of that predicted for a modified Newtonian pressure distribution. The ratio of the square root of the velocity gradient at the stagnation point of the blunt-nose model to the hemispherical-nose model was 0.67 for the same test condition. This value is the same as that given in reference 9 for the two model shapes.

A comparison of the measured pressure distribution data for both model shapes and the measured heating-rate data for the hemisphere-cylinder model indicates that models up to 1 inch (2.5 cm) in diameter can be tested in the 1-inch (2.5-cm) nozzle of the Mach 2 system with flow conditions acceptable for study of the aerothermal response of materials in the stagnation region.

### Range of Aerodynamic Parameters

In table VII are listed some aerodynamic parameters over the range of fire-on settings for the normal operating chamber pressures of 115 and 165 psia (0.79 and 1.14 $MN/m^2$). The parameters are for the 1-inch (2.5-cm) nozzle at a distance of 0.50 inch (1.27 cm) from the nozzle exit. Since the 1/2- and 3/4-inch (1.3- and 1.9-cm) nozzles are very similar to the 1-inch (2.5-cm) nozzle, the values in table VII can be used as estimates for the parameters in the two smaller nozzles. The measured data and references 7, 8, and 13 were used in the preparation of table VII.

## CONCLUDING REMARKS

A Mach 2 nozzle system has been installed in the Langley 11-inch ceramic-heated tunnel to fit interchangeably with existing Mach 4 and Mach 6 systems and the significant operating parameters of the Mach 2 system have been measured. The results of tests to evaluate the suitability of this system for materials research have shown that test times up to 660 seconds can be achieved with only a slight decay of initial total temperature for the normal operating range at chamber pressures of 115 to 165 psia (0.79 to 1.14 $MN/m^2$). The total temperature of the airstream was measured at five standard fire-on settings and was in the range of 2100° R to 4000° R (1170° K to 2220° K). The temperature decrease with test time was linear with an average decrease of approximately 200° R (110° K) in 600 seconds. Low contamination of the test stream by dust from the pebble bed has been demonstrated under certain operating conditions. This contamination, as

measured by its effect on graphite models, is such that it can be neglected on a significant number of experimental programs including material studies. Also, the comparison in pressure, heating-rate, and shear distributions indicates the suitability of material response tests at the stagnation region of a model.

The results presented in this paper can be used to determine the applicability of the Mach 2 system of the Langley 11-inch ceramic-heated tunnel for an experimental program and to select the desired operating conditions.

Langley Research Center,
National Aeronautics and Space Administration,
Langley Station, Hampton, Va., June 4, 1968,
129-03-02-03-23.

## APPENDIX A

## CONVERSION OF U.S. CUSTOMARY UNITS TO SI UNITS

The International System of Units, abbreviated SI (Systeme International), was adopted in 1960 by the Eleventh General Conference on Weights and Measures held in Paris, France. Conversion factors required for units used herein are given in the following table:

| Physical quantity | U.S. Customary Unit | Conversion factor (*) | SI Unit |
|---|---|---|---|
| Aerodynamic shear | $lbf/ft^2$ | 47.88 | $N/m^2$ |
| Density | $lbm/ft^3$ | 16.018 | $kg/m^3$ |
| Enthalpy | Btu/lbm | $2.324 \times 10^3$ | J/kg |
| Heat-transfer coefficient | $Btu/ft^2\text{-sec-}^oR$ | $2.045 \times 10^4$ | $W/m^2\text{-}^oK$ |
| Heating rate | $Btu/ft^2\text{-sec}$ | $1.135 \times 10^4$ | $W/m^2$ |
| Length | ft | 0.3048 | m |
| | in. | 0.0254 | m |
| Pressure | $psia(lbf/in^2)$ | $6.895 \times 10^3$ | $N/m^2$ |
| Reynolds number per unit length | $ft^{-1}$ | 3.28 | $m^{-1}$ |
| Specific heat | $Btu/lbm\text{-}^oR$ | $4.18 \times 10^3$ | $J/kg\text{-}^oK$ |
| Temperature | $^oR$ | 5/9 | $^oK$ |
| Velocity | ft/sec | 0.3048 | m/s |

*Multiply value given in U.S. Customary Unit by conversion factor to obtain equivalent value of SI Unit.

Prefixes to indicate multiples of units are as follows:

| Prefix | Multiple |
|---|---|
| mega (M) | $10^6$ |
| kilo (k) | $10^3$ |
| centi (c) | $10^{-2}$ |

## APPENDIX B

## METHOD OF CALCULATING THE THERMOCOUPLE RADIATION CORRECTION

The following equation is taken from reference 5 for the radiation correction when the thermocouple has reached equilibrium:

$$T_t - T_{w,e} = \frac{\sigma \epsilon_w}{h}\left(T_{w,e}^4 - T_s^4\right) \tag{1}$$

where

$T_t$ airstream total temperature, $^oR$ ($^oK$)

$T_{w,e}$ thermocouple equilibrium temperature, $^oR$ ($^oK$)

$T_s$ shield temperature, $^oR$ ($^oK$)

$\sigma$ Stefan-Boltzmann constant, $4.81 \times 10^{-13}$ Btu/ft$^2$-$^oR^4$-sec ($5.669 \times 10^{-8}$ W/m$^2$-$^oK^4$)

$\epsilon_w$ emissivity of thermocouple wire

h heat-transfer coefficient to thermocouple wire, Btu/ft$^2$-$^oR$-sec (W/m$^2$-$^oK$)

The term $T_t - T_{w,e}$ is the radiation correction.

The heat-transfer coefficient was calculated from experimental data taken from the transient portion of the thermocouple reading. The following equation for the heat-transfer equation is from reference 14:

$$h = \frac{d_w \rho_w C_w}{4\left(T_t - T_{w,i}\right)} \frac{dT_{w,i}}{dt} \tag{2}$$

where

$d_w$ diameter of thermocouple wire, ft (m)

$\rho_w$ density of thermocouple wire, lbm/ft$^3$ (kg/m$^3$)

## APPENDIX B

$C_w$ specific heat of thermocouple wire, Btu/lbm-$^oR$ (J/kg-$^oK$)

$T_{w,i}$ thermocouple temperature at time "i", $^oR$ ($^oK$)

$dT_{w,i}/dt$ time rate of change of thermocouple temperature at time i, $^oR$/sec ($^oK$/s)

The time rate of temperature change $dT_{w,i}/dt$ and the temperature $T_{w,i}$ at time i during the transient condition was measured from the temperature trace as shown in the following sketch:

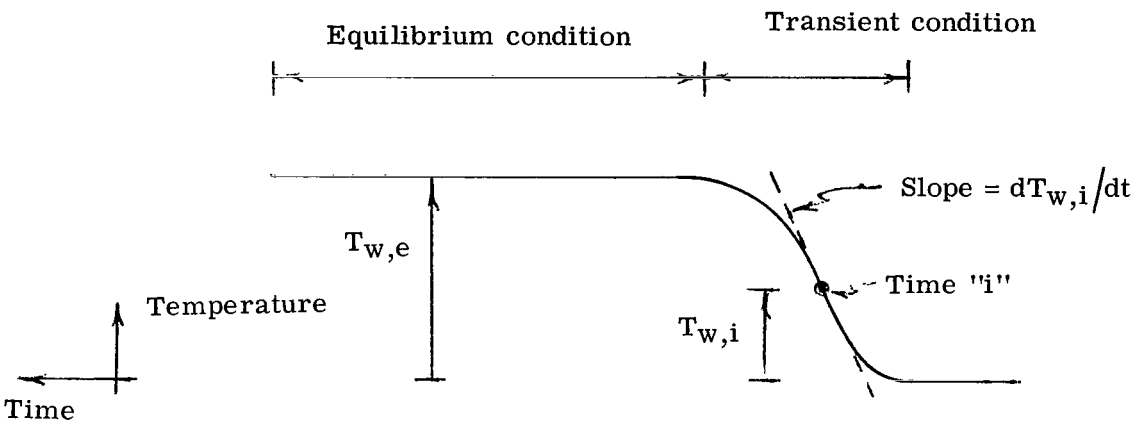


Since it is necessary to know the jet airstream total temperature $T_t$ before using equation (2), a reiterative process is used between equations (1) and (2) to calculate the radiation correction.

The radiation correction was calculated for each insertion during a test; however, the average correction for the entire test was used in determing the total temperature of each insertion of that particular test. For those designs without a shield thermocouple, the radiation correction was calculated by an assumed shield temperature based on knowledge obtained from the designs with a shield thermocouple.

## REFERENCES


1. Trout, Otto F., Jr.: Design, Operation, and Testing Capabilities of the Langley 11-Inch Ceramic-Heated Tunnel. NASA TN D-1598, 1963.

2. Mechtly, E. A.: The International System of Units – Physical Constants and Conversion Factors. NASA SP-7012, 1964.

3. Midden, Raymond E.; and Cocke, Bennie W., Jr.: Diffuser Performance of a Mach 6 Open-Jet Tunnel and Model-Blockage Effects at Stagnation Temperatures to 3,600° F. NASA TN D-2384, 1964.

4. Buckley, John D.; and Cocke, Bennie W., Jr.: Evaluation of Selected Refractory Oxide Materials for Use in High-Temperature Pebble-Bed Wind-Tunnel Heat Exchangers. NASA TN D-2493, 1964.

5. Moffat, Robert J.: Gas Temperature Measurement. Temperature – Its Measurement and Control in Science and Industry, Vol. 3, Pt. 2, Reinhold Pub. Corp., c.1962, pp. 553-571.

6. Gardon, Robert: An Instrument for the Direct Measurement of Intense Thermal Radiation. Rev. Sci. Instr., vol. 24, no. 5, May 1953, pp. 366-370.

7. Ames Research Staff: Equations, Tables, and Charts for Compressible Flow. NACA Rep. 1135, 1953. (Supersedes NACA TN 1428.)

8. Fay, J. A.; and Riddell, F. R.: Theory of Stagnation Point Heat Transfer in Dissociated Air. J. Aeronaut. Sci., vol. 25, no. 2, Feb. 1958, pp. 73-85, 121.

9. Zoby, Ernest V.; and Sullivan, Edward M.: Effects of Corner Radius on Stagnation-Point Velocity Gradients on Blunt Axisymmetric Bodies. NASA TM X-1067, 1965.

10. Cohen, Nathaniel B.: Boundary-Layer Similar Solutions and Correlation Equations for Laminar Heat-Transfer Distribution in Equilibrium Air at Velocities up to 41,100 Feet Per Second. NASA TR R-118, 1961.

11. Beckwith, Ivan E.; and Gallagher, James J.: Heat Transfer and Recovery Temperatures on a Sphere With Laminar, Transitional, and Turbulent Boundary Layers at Mach Numbers of 2.00 and 4.15. NACA TN 4125, 1957.

12. Holloway, Paul F.; and Dunavant, James C.: Heat-Transfer and Pressure Distributions at Mach Numbers of 6.0 and 9.6 Over Two Reentry Configurations for the Five-Stage Scout Vehicle. NASA TN D-1790, 1963.

13. Hansen, C. Frederick: Approximations for the Thermodynamic and Transport Properties of High-Temperature Air. NASA TR R-50, 1959. (Supersedes NACA TN 4150.)

14. Scadron, Marvin D.; and Warshawsky, Isidore: Experimental Determination of Time Constants and Nusselt Numbers for Bare-Wire Thermocouples in High-Velocity Air Streams and Analytic Approximation of Conduction and Radiation Errors. NACA TN 2599, 1952.

TABLE I. - NOZZLE COORDINATES DOWNSTREAM OF THROAT

(a) U. S. Customary Units

| 1-inch nozzle | | 3/4-inch nozzle | | 1/2-inch nozzle | |
|---|---|---|---|---|---|
| Axial distance, in. | Radial distance, in. | Axial distance, in. | Radial distance, in. | Axial distance, in. | Radial distance, in. |
| 0.000 | 0.503 | 0.000 | 0.382 | 0.000 | 0.291 |
| .047 | .509 | .035 | .386 | .027 | .294 |
| .092 | .516 | .069 | .391 | .053 | .298 |
| .138 | .522 | .105 | .396 | .080 | .302 |
| .185 | .529 | .140 | .402 | .107 | .306 |
| .277 | .541 | .210 | .411 | .160 | .313 |
| .370 | .554 | .281 | .420 | .214 | .320 |
| .462 | .564 | .350 | .429 | .267 | .326 |
| .554 | .574 | .420 | .436 | .320 | .332 |
| .647 | .583 | .491 | .442 | .374 | .337 |
| .739 | .593 | .560 | .450 | .427 | .343 |
| .832 | .602 | .631 | .457 | .481 | .348 |
| .924 | .609 | .701 | .462 | .534 | .352 |
| 1.016 | .616 | .770 | .467 | .587 | .356 |
| 1.109 | .623 | .841 | .472 | .641 | .360 |
| 1.201 | .630 | .910 | .477 | .694 | .364 |
| 1.294 | .637 | .916 | .483 | .748 | .368 |
| 1.386 | .642 | 1.051 | .487 | .801 | .371 |
| 1.477 | .645 | 1.121 | .489 | .854 | .373 |
| 1.571 | .650 | 1.191 | .493 | .908 | .376 |
| 1.663 | .654 | 1.261 | .496 | .961 | .378 |
| 1.756 | .656 | 1.332 | .497 | 1.015 | .379 |
| 1.845 | .657 | 1.401 | .499 | 1.068 | .380 |
| 1.939 | .659 | 1.500 | .500 | 1.121 | .381 |

(b) SI Units

| 2.5 cm nozzle | | 1.9 cm nozzle | | 1.3 cm nozzle | |
|---|---|---|---|---|---|
| Axial distance, cm | Radial distance, cm | Axial distance, cm | Radial distance, cm | Axial distance, cm | Radial distance, cm |
| 0.000 | 1.278 | 0.000 | 0.970 | 0.000 | 0.739 |
| .119 | 1.293 | .089 | .980 | .069 | .747 |
| .234 | 1.311 | .175 | .993 | .135 | .757 |
| .351 | 1.326 | .267 | 1.006 | .203 | .767 |
| .470 | 1.344 | .356 | 1.021 | .272 | .777 |
| .704 | 1.374 | .534 | 1.042 | .406 | .795 |
| .940 | 1.407 | .714 | 1.066 | .544 | .813 |
| 1.171 | 1.432 | .889 | 1.089 | .678 | .828 |
| 1.407 | 1.468 | 1.066 | 1.107 | .813 | .843 |
| 1.644 | 1.481 | 1.247 | 1.123 | .950 | .856 |
| 1.877 | 1.506 | 1.423 | 1.143 | 1.075 | .871 |
| 2.112 | 1.529 | 1.603 | 1.161 | 1.222 | .884 |
| 2.347 | 1.547 | 1.781 | 1.174 | 1.356 | .894 |
| 2.581 | 1.564 | 1.956 | 1.186 | 1.491 | .904 |
| 2.818 | 1.582 | 2.136 | 1.199 | 1.628 | .914 |
| 3.050 | 1.601 | 2.311 | 1.211 | 1.763 | .924 |
| 3.288 | 1.618 | 2.352 | 1.226 | 1.900 | .934 |
| 3.520 | 1.631 | 2.669 | 1.237 | 2.034 | .942 |
| 3.752 | 1.638 | 2.848 | 1.242 | 2.169 | .948 |
| 3.990 | 1.651 | 3.027 | 1.252 | 2.308 | .955 |
| 4.223 | 1.661 | 3.202 | 1.260 | 2.440 | .960 |
| 4.460 | 1.666 | 3.382 | 1.262 | 2.578 | .962 |
| 4.687 | 1.669 | 3.559 | 1.268 | 2.712 | .965 |
| 4.923 | 1.674 | 3.810 | 1.270 | 2.849 | .968 |

TABLE II.- RESULTS OF THE DAMAGE TO GRAPHITE MODELS DUE TO AIRSTREAM CONTAMINATION IN THE MACH 2 NOZZLE SYSTEM

[Measurements made before a bed cleaning with a cold bed and a chamber pressure of 115 psia (0.79 $MN/m^2$). Models are 0.500 inch (1.27 cm) diameter hemispheres.]

| Nozzle | Exposure time, seconds | Weight loss, grams | |
|---|---|---|---|
| | | Complete model | Center plug |
| 1-inch (2.5 cm) | 30 | 0.0069 | 0.0005 |
| 1-inch (2.5 cm) | 240 | 0.0247 | 0.0021 |
| 3/4-inch (1.9 cm) | 30 | 0.0012 | 0.0001 |
| 3/4-inch (1.9 cm) | 240 | 0.0022 | 0.0004 |
| 1/2-inch (1.3 cm) | 30 | 0.0012 | 0.0000 |
| 1/2-inch (1.3 cm) | 240 | 0.0012 | 0.0002 |

TABLE III. - RESULTS OF FIRST SERIES OF TOTAL TEMPERATURE MEASUREMENTS

(a) U. S. Customary Units

[Measurements made in the 1-inch nozzle at a chamber pressure of 115 psia and at a distance of 0.25 inches from exit plane of nozzle. Test series made after a cleaning of the pebble bed.]

| Thermocouple design number | Pebble bed temperature, °R | | | | Airstream total temperature at time indicated, °R | | | | | | | Average total temperature, °R | Radiation correction, °R |
|---|---|---|---|---|---|---|---|---|---|---|---|---|---|
| | Fire on | Fire off | After run | Average bed | 0 | 60 sec | 120 sec | 180 sec | 240 sec | 300 sec | 360 sec | | |
| 1 | 3485 | 3370 | 3230 | 3300 | 3177 | 3203 | 3168 | 3167 | 3144 | - | - | 3170 | 55 |
| 2 | 3500 | 3360 | 3230 | 3295 | 3256 | 3236 | 3213 | 3199 | 3211 | 3188 | 3186 | 3210 | 78 |
| 2 | 4070 | 3980 | 3760 | 3870 | 3621 | 3612 | 3612 | 3579 | 3556 | 3564 | - | 3590 | 89 |
| 2 | 4460 | 4320 | 3980 | 4150 | 3959 | 3944 | 3881 | 3898 | 3864 | 3891 | 3874 | 3880 | 129 |
| 3 | 3480 | 3340 | 3240 | 3290 | 3148 | 3125 | 3174 | 3181 | 3132 | 3174 | - | 3160 | 0 |
| 4 | 2500 | 2440 | 2225 | 2333 | 2242 | 2235 | 2188 | 2164 | 2144 | 2119 | 2099 | 2170 | 6 |
| 4 | 2970 | 2900 | 2660 | 2780 | 2762 | 2742 | 2705 | 2699 | 2667 | 2641 | 2609 | 2690 | 8 |
| 4 | 3485 | 3375 | 3240 | 3308 | 3106 | 3098 | 3087 | 3105 | 3105 | 3105 | - | 3100 | 31 |
| 5 | 2485 | 2470 | 2360 | 2415 | 2333 | 2321 | 2317 | 2312 | 2301 | 2309 | 2288 | 2310 | 12 |
| 5 | 3050 | 2980 | 2830 | 2905 | 2784 | 2763 | 2649 | 2594 | 2552 | 2547 | 2518 | 2630 | 18 |
| 5 | 3500 | 3390 | 3230 | 3310 | 3248 | 3222 | 3201 | 3172 | 3166 | 3096 | 3022 | 3160 | 41 |
| 5 | 4010 | 3860 | 3680 | 3770 | 3648 | 3627 | 3598 | 3571 | 3598 | 3554 | 3498 | 3585 | 86 |
| 5 | 4470 | 4360 | 4000 | 4180 | 3933 | 3915 | - | - | - | - | - | - | 85 |
| 6 | 2600 | 2500 | 2360 | 2440 | 2379 | 2328 | 2311 | 2275 | 2275 | 2242 | 2204 | 2290 | 12 |
| 6 | 2970 | 2910 | 2730 | 2820 | 2704 | 2667 | 2639 | 2626 | 2600 | 2579 | 2535 | 2620 | 21 |
| 6 | 3485 | 3395 | 3175 | 3285 | 3121 | 3086 | 3101 | 3052 | 3012 | 3012 | 2974 | 3050 | 37 |
| 6 | 3970 | 3870 | 3640 | 3755 | 3545 | 3469 | 3443 | 3414 | 3421 | 3397 | 3370 | 3450 | 75 |
| 6 | 4460 | 4310 | 4010 | 4160 | 4058 | 3969 | 3901 | 3919 | - | - | - | 3960 | 137 |

TABLE III. - RESULTS OF FIRST SERIES OF TOTAL TEMPERATURE MEASUREMENTS - CONCLUDED

(b) SI Units

[Measurements made in the 2.5 centimeter nozzle at a chamber pressure of 0.79 $MN/m^2$ and at a distance of 0.63 centimeters from exit plane of nozzle. Test series made after a cleaning of the pebble bed.]

| Thermocouple design number | Pebble bed temperature, °K | | | | Airstream total temperature at time indicated, °K | | | | | | | Average total temperature, °K | Radiation correction, °K |
|---|---|---|---|---|---|---|---|---|---|---|---|---|---|
| | Fire on | Fire off | After run | Average bed | 0 | 60 sec | 120 sec | 180 sec | 240 sec | 300 sec | 360 sec | | |
| 1 | 1935 | 1873 | 1794 | 1833 | 1764 | 1779 | 1759 | 1753 | 1747 | - | - | 1760 | 30.5 |
| 2 | 1944 | 1866 | 1794 | 1830 | 1808 | 1797 | 1785 | 1776 | 1783 | 1770 | 1769 | 1780 | 43.3 |
| 2 | 2261 | 2211 | 2088 | 2150 | 2011 | 2008 | 2008 | 1987 | 1975 | 1980 | - | 1995 | 49.4 |
| 2 | 2478 | 2400 | 2217 | 2304 | 2199 | 2191 | 2157 | 2165 | 2147 | 2162 | 2152 | 2155 | 71.6 |
| 3 | 1933 | 1855 | 1800 | 1828 | 1748 | 1736 | 1763 | 1767 | 1740 | 1763 | - | 1755 | 0 |
| 4 | 2388 | 1356 | 1236 | 1296 | 1246 | 1242 | 1215 | 1203 | 1192 | 1177 | 1166 | 1205 | 3.3 |
| 4 | 1650 | 1611 | 1478 | 1544 | 1534 | 1524 | 1503 | 1499 | 1481 | 1467 | 1448 | 1495 | 4.4 |
| 4 | 1936 | 1876 | 1800 | 1837 | 1725 | 1720 | 1714 | 1725 | 1725 | 1725 | - | 1720 | 17.2 |
| 5 | 1381 | 1373 | 1311 | 1342 | 1296 | 1289 | 1287 | 1284 | 1278 | 1283 | 1270 | 1285 | 6.7 |
| 5 | 1694 | 1656 | 1572 | 1614 | 1546 | 1535 | 1472 | 1441 | 1418 | 1414 | 1398 | 1460 | 10.0 |
| 5 | 1945 | 1883 | 1794 | 1838 | 1804 | 1790 | 1778 | 1762 | 1758 | 1720 | 1679 | 1755 | 22.8 |
| 5 | 2228 | 2144 | 2044 | 2094 | 2025 | 2015 | 1998 | 1984 | 1998 | 1975 | 1943 | 1990 | 47.8 |
| 5 | 2482 | 2422 | 2222 | 2322 | 2185 | 2174 | - | - | - | - | - | - | 47.2 |
| 6 | 1444 | 1389 | 1311 | 1356 | 1321 | 1293 | 1284 | 1264 | 1264 | 1246 | 1224 | 1270 | 6.7 |
| 6 | 1650 | 1616 | 1516 | 1566 | 1503 | 1481 | 1465 | 1459 | 1444 | 1433 | 1408 | 1455 | 11.7 |
| 6 | 1936 | 1886 | 1754 | 1825 | 1734 | 1714 | 1723 | 1695 | 1674 | 1674 | 1653 | 1695 | 20.6 |
| 6 | 2205 | 2150 | 2022 | 2086 | 1969 | 1927 | 1913 | 1896 | 1901 | 1886 | 1872 | 1914 | 41.7 |
| 6 | 2478 | 2394 | 2228 | 2311 | 2253 | 2204 | 2168 | 2178 | - | - | - | 2200 | 76.2 |

TABLE IV. - RESULTS OF SECOND SERIES OF TOTAL TEMPERATURE MEASUREMENTS

[Measurements made in the 1-inch (2.5 cm) nozzle at a distance of 0.50 inches (1.27 cm) from exit plane of nozzle. Thermocouple design no. 7 used for the measurements. Test series made before a cleaning of the pebble bed.]

(a) U. S. Customary Units

| Fire-on temperature, °R | Chamber pressure, psia | Total temperature at time indicated, °R | | | | | | | | | | | |
|---|---|---|---|---|---|---|---|---|---|---|---|---|---|
| | | 0 | 60 sec | 120 sec | 180 sec | 240 sec | 300 sec | 360 sec | 420 sec | 480 sec | 540 sec | 600 sec | 660 sec |
| 2460 | 115 | 2251 | 2224 | 2200 | 2200 | 2167 | 2167 | 2149 | 2149 | 2132 | 2116 | - | - |
| 2460 | 165 | 2197 | 2146 | 2146 | 2129 | 2097 | 2062 | 2045 | 2062 | 2062 | 2062 | - | - |
| 3460 | 115 | 3061 | 3045 | 2986 | 2984 | 2949 | 2930 | 2912 | 2877 | 2823 | 2823 | 2804 | 2776 |
| 3500 | 165 | 3106 | 3087 | 3049 | 3030 | 2996 | 2981 | 2905 | 2887 | 2833 | 2815 | 2798 | 2780 |
| 4470 | 115 | - | 4050 | 4025 | 4002 | 3956 | 3899 | 3807 | 3761 | 3761 | 3703 | 3657 | 3680 |
| 4490 | 165 | - | 4165 | 4095 | 4050 | 4015 | 4025 | 4015 | 4050 | 3992 | 3922 | 3876 | 3853 |

(b) SI Units

| Fire-on temperature, °K | Chamber pressure, $MN/m^2$ | Total temperature at time indicated, °K | | | | | | | | | | | |
|---|---|---|---|---|---|---|---|---|---|---|---|---|---|
| | | 0 | 30 sec | 60 sec | 180 sec | 240 sec | 300 sec | 360 sec | 420 sec | 480 sec | 540 sec | 600 sec | 660 sec |
| 1366 | .79 | 1251 | 1236 | 1222 | 1222 | 1203 | 1203 | 1194 | 1194 | 1185 | 1175 | - | - |
| 1366 | 1.14 | 1219 | 1192 | 1192 | 1183 | 1164 | 1146 | 1136 | 1146 | 1146 | 1146 | - | - |
| 1922 | .79 | 1701 | 1692 | 1658 | 1657 | 1638 | 1627 | 1618 | 1597 | 1568 | 1568 | 1558 | 1542 |
| 1944 | 1.14 | 1726 | 1714 | 1693 | 1683 | 1664 | 1656 | 1614 | 1604 | 1574 | 1564 | 1554 | 1544 |
| 2482 | .79 | - | 2250 | 2237 | 2223 | 2198 | 2166 | 2114 | 2089 | 2089 | 2058 | 2031 | 2043 |
| 2493 | 1.14 | - | 2313 | 2275 | 2250 | 2230 | 2236 | 2230 | 2250 | 2219 | 2219 | 2152 | 2141 |

TABLE V.- RESULTS OF TOTAL-PRESSURE MEASUREMENTS

(a) U. S. Customary Units

| Test | Nominal throat diameter, in. | Distance from exit plane of nozzle, in. | Probe diameter, in. | $T_t$, °R | $p_c$, psia | $p_{t,2}$, psia | $p_{t,2}/p_c$ | Mach number |
|---|---|---|---|---|---|---|---|---|
| 1 | 1 | .50 | 1.000 | 3920 | 114.2 | 75.7 | 0.662 | 2.07 |
| | | | | | 162.7 | 109.7 | .674 | 2.05 |
| 2 | 1 | .50 | 1.000 | 3150 | 113.7 | 75.2 | .661 | 2.08 |
| | | | | | 164.2 | 109.7 | .668 | 2.06 |
| 3 | 1 | .50 | 1.000 | 2760 | 114.2 | 75.7 | .662 | 2.08 |
| | | | | | 164.2 | 109.7 | .668 | 2.07 |
| 4 | 1 | .50 | 1.000 | 2350 | 115.7 | 76.7 | .663 | 2.09 |
| | | | | | 164.7 | 109.7 | .666 | 2.08 |
| 5 | 1 | .50 | .500 | 3950 | 108.2 | 70.7 | .653 | 2.09 |
| | | | | | 156.2 | 101.2 | .647 | 2.10 |
| 6 | 1 | .50 | .500 | 3950 | 115.5 | 73.7 | .638 | 2.12 |
| | | | | | 163.5 | 105.2 | .639 | 2.12 |
| 7 | 1 | .50 | .375 | 3950 | 127.2 | 85.2 | .660 | 2.08 |
| | | | | | 161.7 | 106.2 | | |
| | | | | | 174.7 | 114.7 | | |
| | | | | | 224.7 | 147.7 | | |
| | | | | | 284.7 | 187.7 | | |
| | | | | | 329.7 | 218.2 | | |
| 8 | 1 | .12 | .375 | 3950 | 112.2 | 79.7 | .711 | 1.98 |
| | | | | | 162.7 | 116.2 | .715 | 1.97 |
| 9 | 1 | 1.00 | .375 | 3950 | 113.7 | 70.5 | .620 | 2.16 |
| | | | | | 161.7 | 102.2 | .635 | 2.13 |
| 10 | 1 | 1.50 | .375 | 3950 | 113.7 | 77.0 | .678 | 2.05 |
| | | | | | 162.7 | 60.1 | .370 | 2.74 |
| 11 | 1 | 2.00 | .375 | 3950 | 113.7 | 85.7 | .755 | 1.89 |
| | | | | | 161.7 | 52.7 | .326 | 2.87 |
| 12 | 1 | 2.50 | .375 | 3950 | 112.3 | 83.7 | .745 | 1.91 |
| | | | | | 161.2 | 99.0 | .588 | 2.23 |
| 13 | 3/4 | .50 | .375 | 3950 | 119.7 | 79.7 | .673 | 2.05 |
| | | | | | 162.7 | 107.7 | | |
| | | | | | 231.7 | 154.7 | | |
| | | | | | 271.7 | 181.7 | | |
| | | | | | 319.7 | 215.7 | | |
| 14 | 1/2 | .12 | .500 | 3950 | 113.7 | 80.2 | .710 | 1.98 |
| | | | | | 162.2 | 115.2 | | |
| 15 | 1/2 | .50 | .500 | 3950 | 112.7 | 74.7 | .664 | 2.07 |
| | | | | | 162.2 | 101.2 | .624 | 2.15 |
| 16 | 1/2 | 1.00 | .500 | 3950 | 113.2 | 77.2 | .682 | 2.03 |
| | | | | | 161.2 | 80.2 | .497 | 2.42 |

TABLE V.- RESULTS OF TOTAL-PRESSURE MEASUREMENTS - Concluded

(b) SI Units

| Test | Nominal throat diameter, cm | Distance from exit plane of nozzle, cm | Probe diameter, cm | $T_t$, °K | $p_c$, MN/m² | $p_{t,2}/p_c$ | $p_{t,2}/p_{t,1}$ | Mach number |
|---|---|---|---|---|---|---|---|---|
| 1 | 2.5 | 1.27 | 2.540 | 2178 | 0.788 | 0.522 | 0.662 | 2.07 |
| | | | | | 1.122 | .756 | .674 | 2.05 |
| 2 | 2.5 | 1.27 | 2.540 | 1750 | .784 | .518 | .661 | 2.08 |
| | | | | | 1.132 | .756 | .668 | 2.06 |
| 3 | 2.5 | 1.27 | 2.540 | 1530 | .788 | .522 | .662 | 2.08 |
| | | | | | 1.132 | .756 | .668 | 2.07 |
| 4 | 2.5 | 1.27 | 2.540 | 1310 | .798 | .529 | .663 | 2.09 |
| | | | | | 1.135 | .756 | .666 | 2.08 |
| 5 | 2.5 | 1.27 | 1.270 | 2195 | .746 | .488 | .653 | 2.09 |
| | | | | | 1.076 | .697 | .647 | 2.10 |
| 6 | 2.5 | 1.27 | 1.270 | 2195 | .796 | .508 | .638 | 2.12 |
| | | | | | 1.126 | .724 | .639 | 2.12 |
| 7 | 2.5 | 1.27 | .953 | 2195 | .877 | .586 | .660 | 2.08 |
| | | | | | 1.115 | .731 | | |
| | | | | | 1.204 | .790 | | |
| | | | | | 1.548 | 1.017 | | |
| | | | | | 1.963 | 1.294 | | |
| | | | | | 2.272 | 1.505 | | |
| 8 | 2.5 | .32 | .953 | 2195 | .773 | .550 | .711 | 1.98 |
| | | | | | 1.122 | .800 | .715 | 1.97 |
| 9 | 2.5 | 2.54 | .953 | 2195 | .784 | .486 | .620 | 2.16 |
| | | | | | 1.115 | .704 | .635 | 2.13 |
| 10 | 2.5 | 3.81 | .953 | 2195 | .784 | .531 | .678 | 2.05 |
| | | | | | 1.122 | .414 | .370 | 2.74 |
| 11 | 2.5 | 5.08 | .953 | 2195 | .784 | .591 | .755 | 1.89 |
| | | | | | 1.115 | .363 | .326 | 2.87 |
| 12 | 2.5 | 6.35 | .953 | 2195 | .774 | .577 | .745 | 1.91 |
| | | | | | 1.111 | .682 | .588 | 2.23 |
| 13 | 1.9 | 1.27 | .953 | 2195 | .825 | .549 | .673 | 2.05 |
| | | | | | 1.122 | .741 | | |
| | | | | | 1.596 | 1.066 | | |
| | | | | | 1.873 | 1.252 | | |
| | | | | | 2.202 | 1.486 | | |
| 14 | 1.3 | .32 | 1.270 | 2195 | .784 | .553 | .710 | 1.98 |
| | | | | | 1.118 | .793 | | |
| 15 | 1.3 | 1.27 | 1.270 | 2195 | .777 | .515 | .664 | 2.07 |
| | | | | | 1.118 | .697 | .624 | 2.15 |
| 16 | 1.3 | 2.54 | 1.270 | 2195 | .779 | .532 | .682 | 2.03 |
| | | | | | 1.111 | .553 | .497 | 2.42 |

TABLE VI.- RESULTS OF STAGNATION-POINT HEATING-RATE MEASUREMENTS

(a) U. S. Customary Units

| Model description | | | Airstream parameters | | | Heating rate, $\dot{q}_s$, Btu/ft$^2$-sec | |
|---|---|---|---|---|---|---|---|
| Calorimeter type | Nose shape | $R_{eff}$, in. | $p_c$, psia | $p_{t,2}$, psia | $T_t$, °R | Measured* | Calculated |
| Thin wall (0.025 in.) | Hemisphere | 0.50 | 120 | 82 | 2260 | 199 | 194 |
| ↓ | ↓ | ↓ | 174 | 119 | 2260 | 230 | 234 |
| ↓ | ↓ | ↓ | 120 | 82 | 3160 | 365 | 308 |
| Thin wall (0.074 in.) | Hemisphere | 0.50 | 115 | 76 | 3160 | 295 | 296 |
| ↓ | ↓ | ↓ | 135 | 89 | 4000 | 420 | 455 |
| ↓ | ↓ | ↓ | 246 | 162 | 4000 | 600 | 612 |
| Continuous reading | Blunt | 1.11 | 123 | 81 | 2260 | 105 $^{120}_{95}$ | 129 |
| ↓ | ↓ | ↓ | 125 | 82 | 2260 | 162 $^{180}_{140}$ | 160 |
| ↓ | ↓ | ↓ | 336 | 222 | 2260 | 235 $^{260}_{215}$ | 215 |
| ↓ | ↓ | ↓ | 232 | 153 | 4000 | 395 $^{430}_{352}$ | 400 |
| ↓ | ↓ | ↓ | 345 | 228 | 4000 | 485 $^{540}_{455}$ | 490 |
| Continuous reading | Flat face | 1.07 | 128 | 84 | 2260 | 120 $^{140}_{110}$ | 135 |
| ↓ | ↓ | ↓ | 129 | 85 | 3160 | 245 $^{270}_{220}$ | 216 |
| ↓ | ↓ | ↓ | 131 | 86 | 4000 | 310 $^{370}_{245}$ | 308 |
| ↓ | ↓ | ↓ | 238 | 157 | 2260 | 350 $^{400}_{315}$ | 293 |
| ↓ | ↓ | ↓ | 238 | 157 | 4000 | 500 $^{560}_{405}$ | 416 |
| ↓ | ↓ | ↓ | 324 | 214 | 4000 | 515 $^{635}_{402}$ | 485 |

*Upper number is maximum value due to fluctuation; lower number is minimum. Main value is the average over the entire reading.

(b) SI Units

| Model description | | | Airstream parameters | | | Heating rate, $\dot{q}_s$, MW/m$^2$ | |
|---|---|---|---|---|---|---|---|
| Calorimeter type | Nose shape | $R_{eff}$, cm | $p_c$, MN/m$^2$ | $p_{t,2}$, MN/m$^2$ | $T_t$, °K | Measured* | Calculated |
| Thin wall (0.064 cm) | Hemisphere | 1.27 | 0.828 | 0.565 | 1255 | 2.26 | 2.20 |
| ↓ | ↓ | ↓ | 1.200 | .821 | 1255 | 2.61 | 2.66 |
| ↓ | ↓ | ↓ | .828 | .565 | 1755 | 4.14 | 3.50 |
| Thin wall (0.188 cm) | Hemisphere | 1.27 | .793 | .524 | 1755 | 3.35 | 3.36 |
| ↓ | ↓ | ↓ | .931 | .614 | 2220 | 4.77 | 5.16 |
| ↓ | ↓ | ↓ | 1.696 | 1.117 | 2220 | 6.81 | 6.94 |
| Continuous reading | Blunt | 2.82 | .848 | .559 | 1255 | 1.14 $^{1.36}_{1.08}$ | 1.46 |
| ↓ | ↓ | ↓ | .862 | .566 | 1255 | 1.84 $^{2.04}_{1.59}$ | 1.82 |
| ↓ | ↓ | ↓ | 2.318 | 1.532 | 1255 | 1.67 $^{2.95}_{2.44}$ | 2.44 |
| ↓ | ↓ | ↓ | 1.600 | 1.055 | 2220 | 4.48 $^{4.88}_{4.00}$ | 4.54 |
| ↓ | ↓ | ↓ | 2.378 | 1.573 | 2220 | 5.50 $^{6.13}_{5.16}$ | 5.56 |
| Continuous reading | Flat face | 2.72 | .882 | .579 | 1255 | 1.36 $^{1.59}_{1.25}$ | 1.53 |
| ↓ | ↓ | ↓ | .890 | .586 | 1755 | 2.78 $^{3.06}_{2.50}$ | 2.45 |
| ↓ | ↓ | ↓ | .903 | .593 | 2220 | 3.52 $^{4.20}_{2.78}$ | 3.50 |
| ↓ | ↓ | ↓ | 1.641 | 1.083 | 1255 | 3.97 $^{4.54}_{3.57}$ | 3.32 |
| ↓ | ↓ | ↓ | 1.641 | 1.083 | 2220 | 5.68 $^{6.36}_{4.60}$ | 4.72 |
| ↓ | ↓ | ↓ | 2.235 | 1.475 | 2220 | 5.84 $^{7.21}_{4.56}$ | 5.50 |

*Upper number is maximum value due to fluctuation; lower number is minimum. Main value is the average over the entire reading.

TABLE VII. RANGE OF AERODYNAMIC PARAMETERS IN THE MACH 2 NOZZLE SYSTEM FOR NORMAL OPERATING PRESSURES

(a) U. S. Customary Units

| Fire-on temperature, $^{o}R$ | 2460. | | 4460 | |
|---|---|---|---|---|
| $p_c$, psia | 115 | 165 | 115 | 165 |
| $T_t$, $^{o}R$ | 2250 | 2250 | 3960 | 3960 |
| $H_t$, Btu/lbm | 570 | 570 | 1080 | 1080 |
| $T_l$, $^{o}R$ | 1280 | 1280 | 2340 | 2340 |
| $V_l$, ft/sec | 3700 | 3700 | 5000 | 5000 |
| $p_{t,2}$, psia | 76 | 109 | 76 | 109 |
| $p_l$, psia | 13 | 19 | 13 | 19 |
| $\rho_l$, lbm/ft$^3$ | .027 | .038 | .015 | .021 |
| $\frac{1}{2}\rho_l V_l^2$, psia | 40 | 56 | 40 | 56 |
| $N_{Re,l}$, ft$^{-1}$ | $4.4\times10^6$ | $6.2\times10^6$ | $2.2\times10^6$ | $3.2\times10^6$ |
| $\dot{q}_s\sqrt{R_{eff}}$, Btu/ft$^3/_2$sec | 38 | 45 | 87 | 103 |

(b) SI Units

| Fire-on temperature, $^{o}K$ | 1370 | | 2480 | |
|---|---|---|---|---|
| $p_c$, MN/m$^2$ | 0.79 | 1.14 | 0.79 | 1.14 |
| $T_t$, $^{o}K$ | 1250 | 1250 | 2200 | 2200 |
| $H_t$, MJ/kg | 1.32 | 1.32 | 2.51 | 2.51 |
| $T_l$, $^{o}K$ | 710 | 710 | 1300 | 1300 |
| $V_l$, m/s | 1130 | 1130 | 1520 | 1520 |
| $p_{t,2}$, MN/m$^2$ | .52 | .75 | .52 | .75 |
| $p_l$, MN/m$^2$ | .09 | .13 | .09 | .13 |
| $\rho_l$, kg/m$^3$ | .434 | .609 | .246 | .336 |
| $\frac{1}{2}\rho_l V_l^2$, MN/m$^2$ | .28 | .39 | .28 | .39 |
| $N_{Re,l}$, m$^{-1}$ | $1.44\times10^7$ | $2.03\times10^7$ | $.72\times10^7$ | $1.05\times10^7$ |
| $\dot{q}\sqrt{R_{eff}}$, MW/m$^{3/2}$ | .24 | .28 | .55 | .65 |

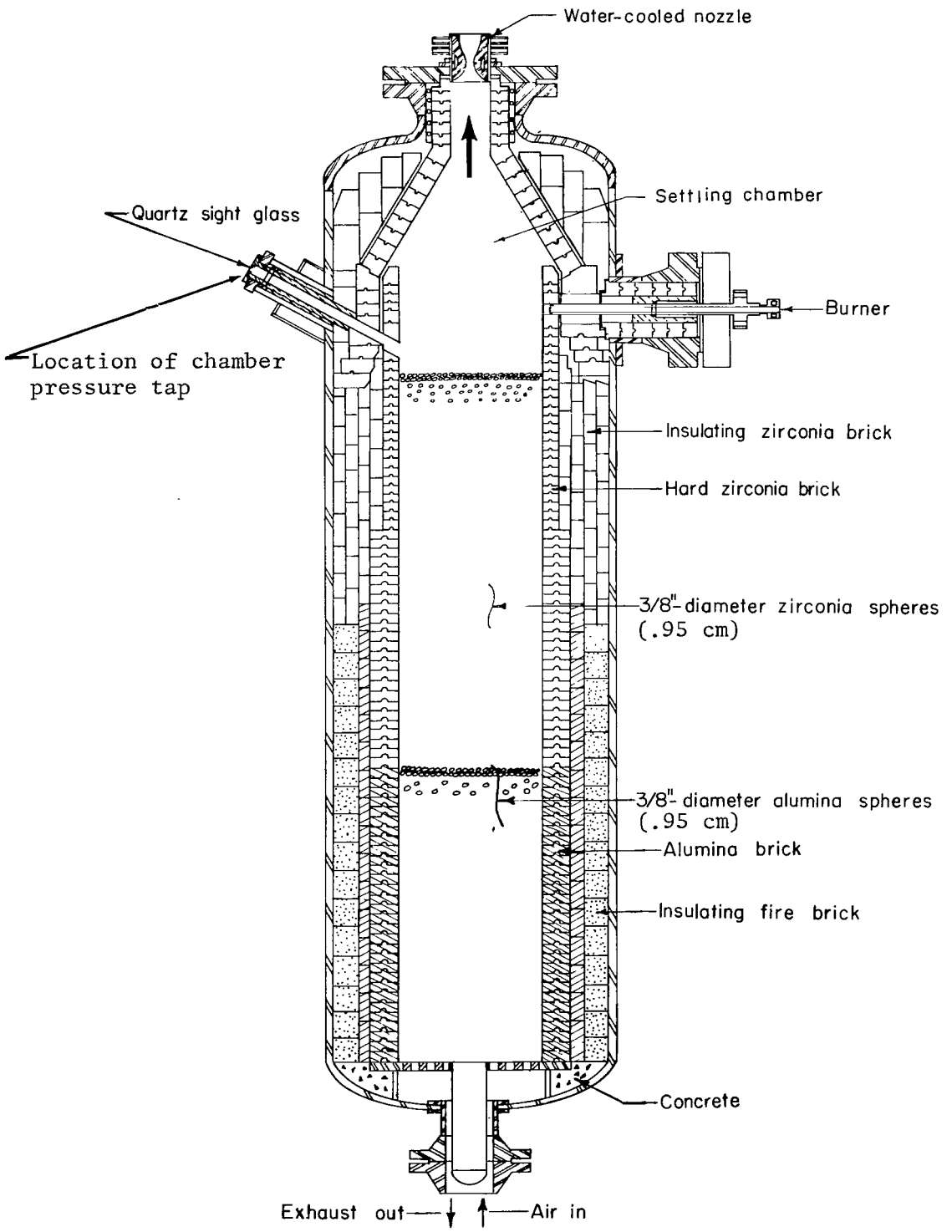


Figure 1.- Components of heat exchanger of Langley 11-inch ceramic-heated tunnel.

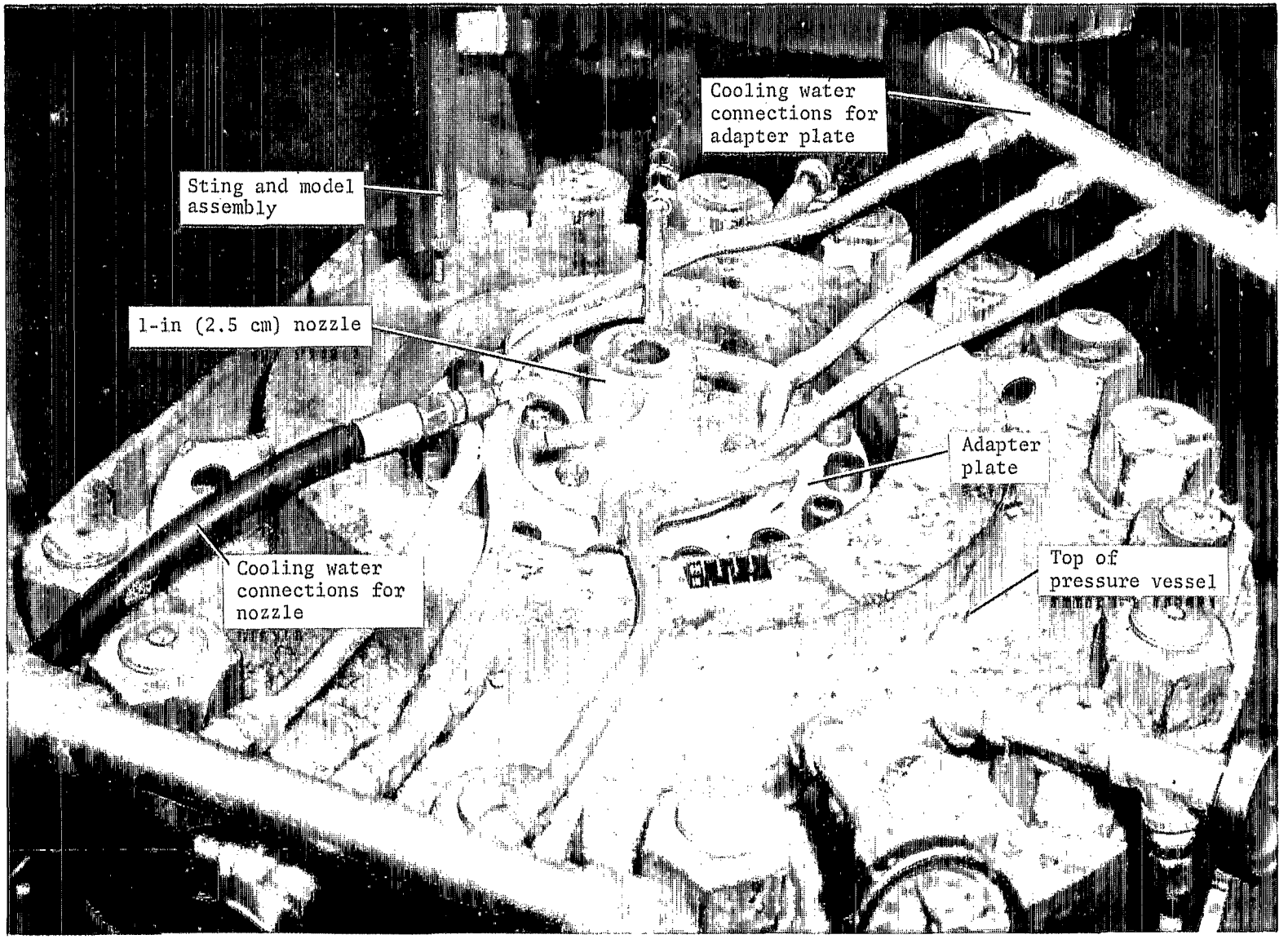


Figure 2.- Photograph of arrangement of Mach 2 nozzle. L-65-7059.1

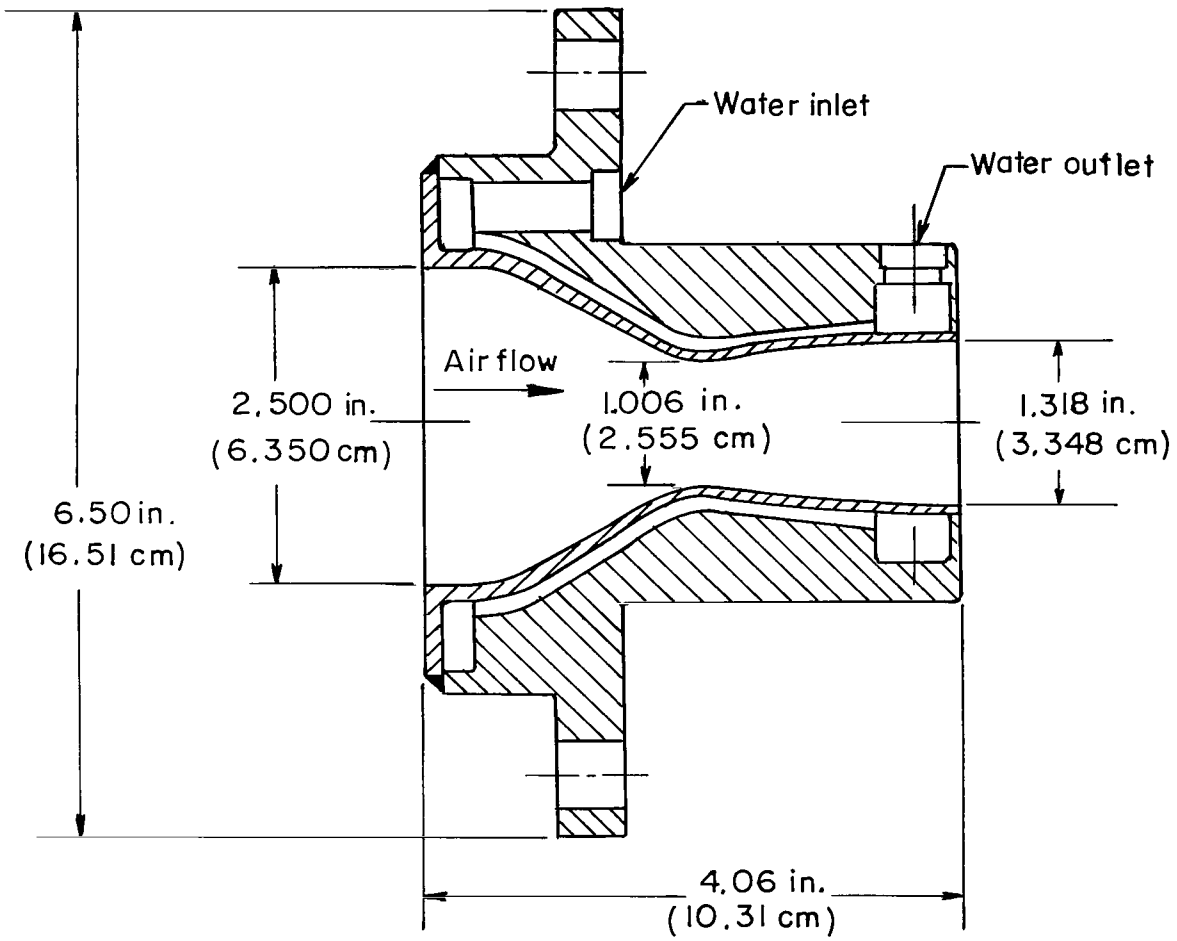


Figure 3.- Section view of 1-inch (2.5-cm) nozzle. Nozzle coordinates listed in table I.

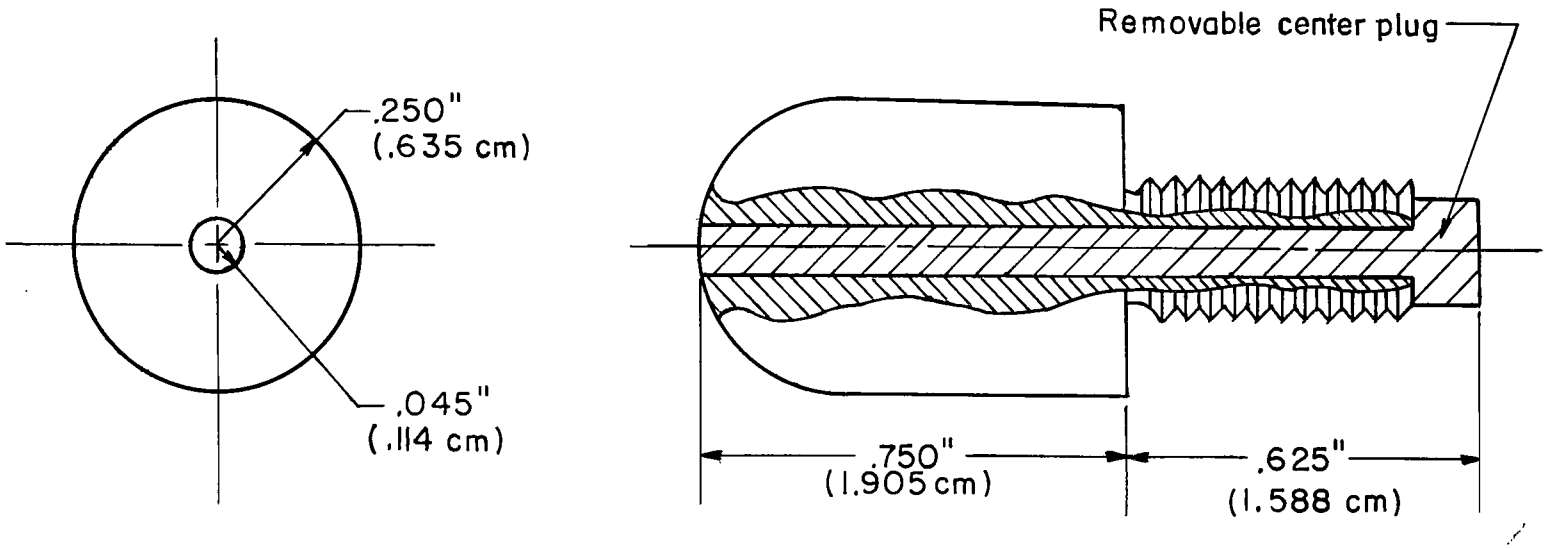


Figure 4.- Details of graphite model used for measurement of effect of stream contamination.

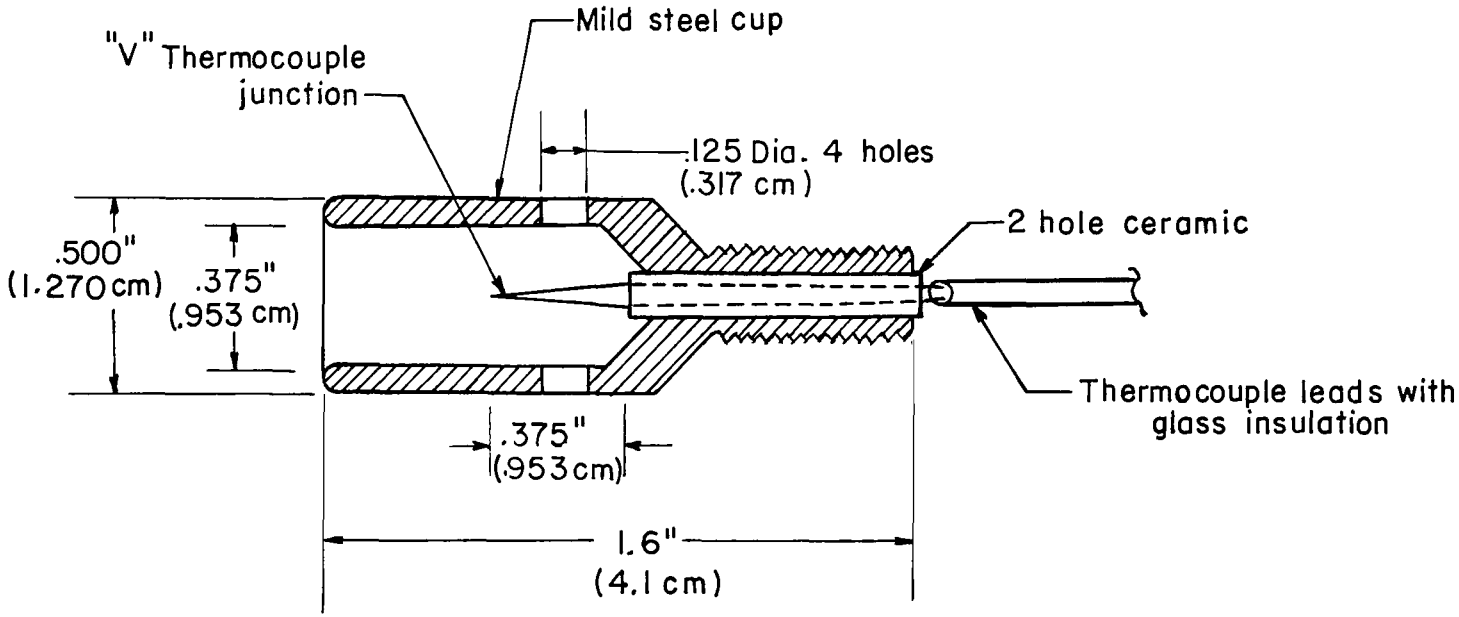


Thermocouple no. 1 – 30 gage Pt-Pt-13-percent Rh wire

Thermocouple no. 2 – 30 gage Ir-Ir – 40-percent Rh wire

(a) Thermocouple designs 1 and 2.

Figure 5.- Details of thermocouple probes.

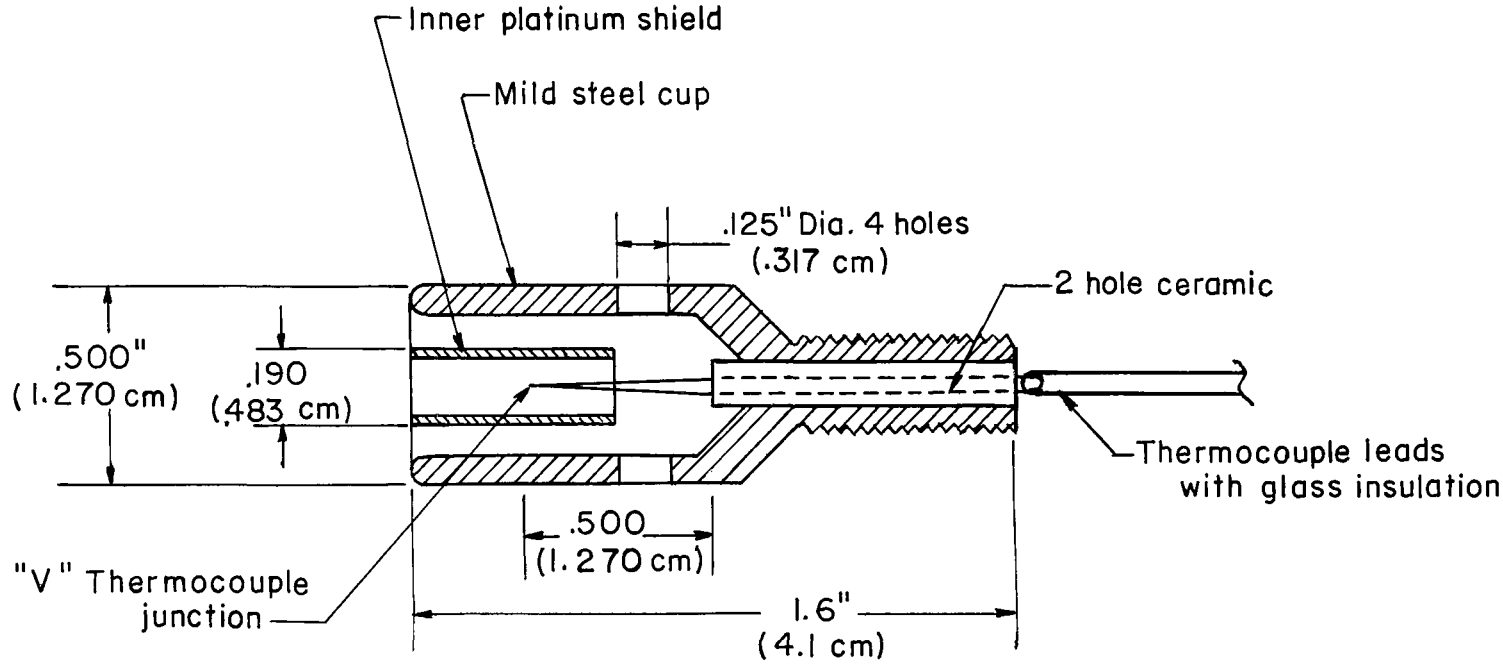


(b) Thermocouple design 3.

Figure 5.- Continued.

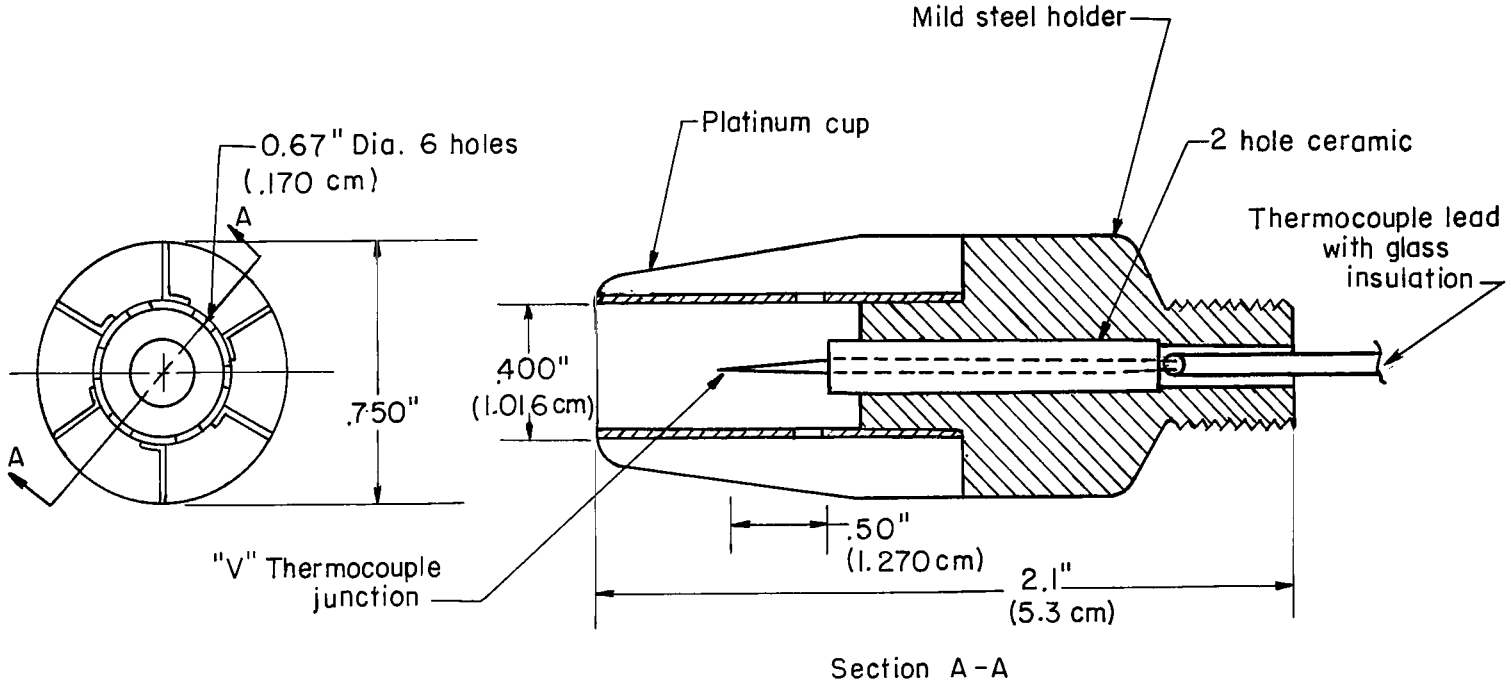


Total temperature thermocouple - 24 gage Pt-Pt-13-percent Rh

(c) Thermocouple design 4.

Figure 5.- Continued.

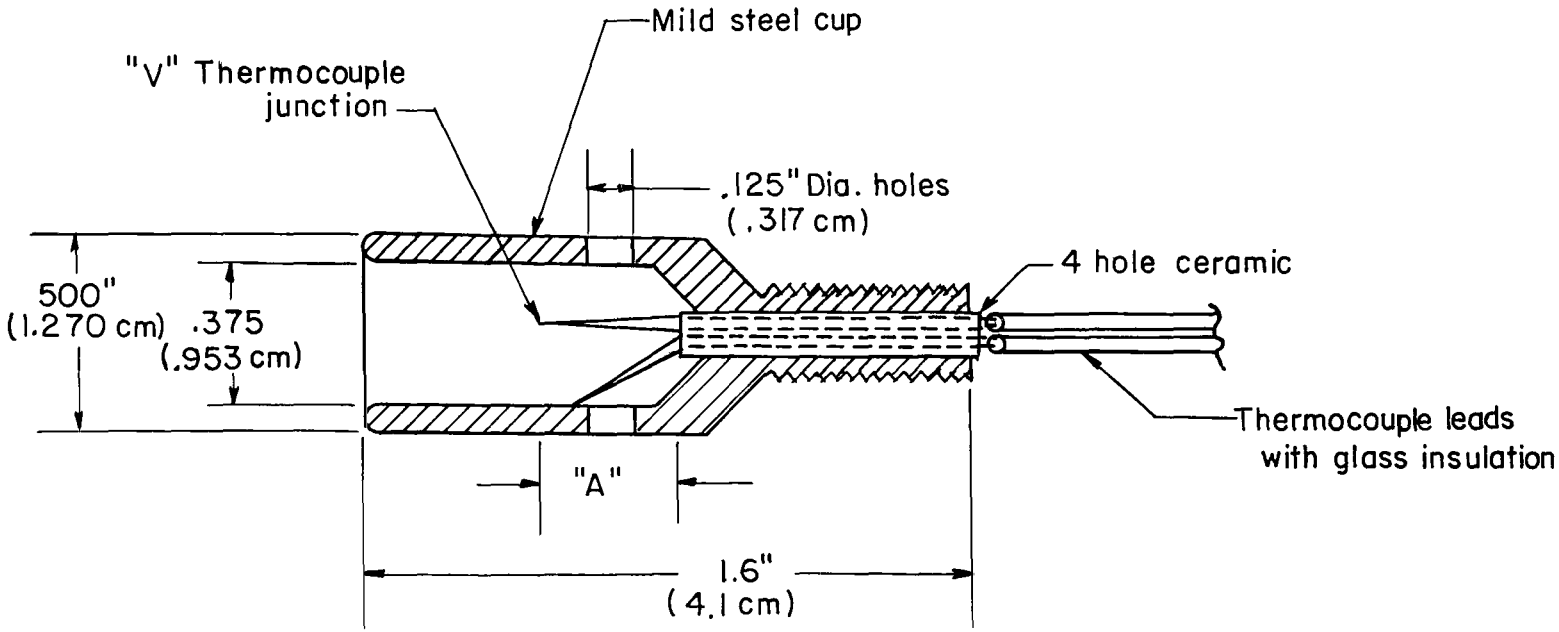


Total temperature thermocouple -30 gage Ir - Ir - 40- percent Rh wire

Shield thermocouple -30 gage Pt-Pt-13-percent Rh wire

Thermocouple no.5 "A" dimension =.375" (.953 cm)

Thermocouple no.6 "A" dimension =.250" (.635 cm)

(d) Thermocouple designs 5 and 6.

Figure 5.- Continued.

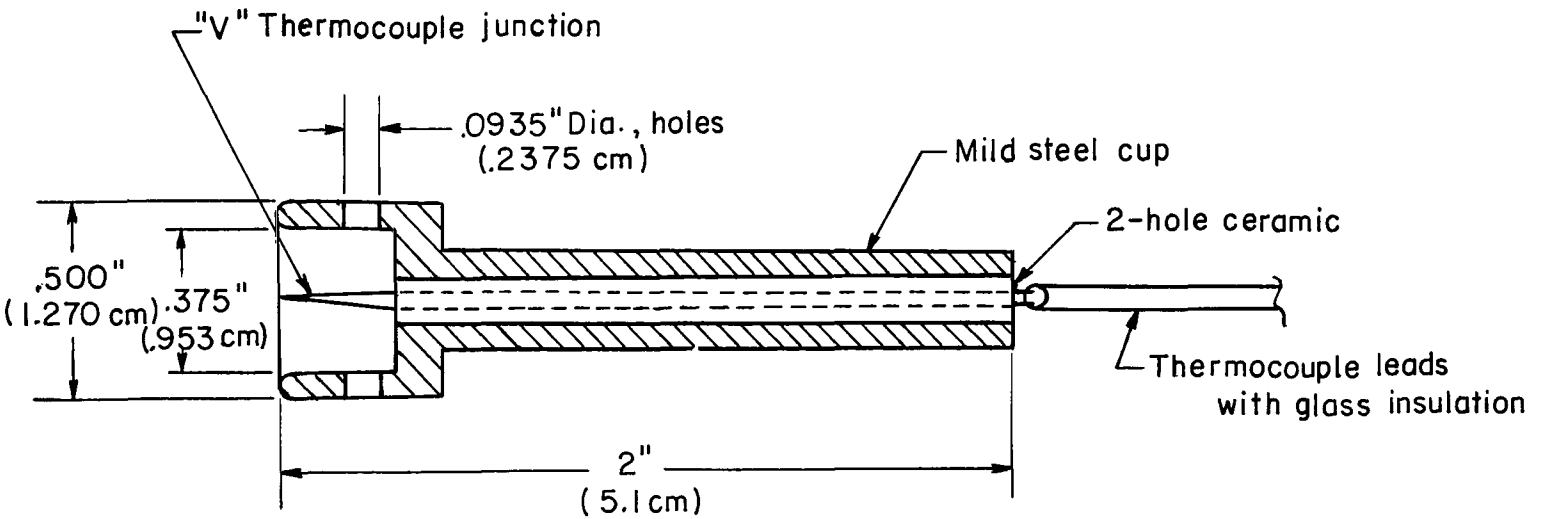


(e) Thermocouple design 7.

Figure 5.- Concluded.

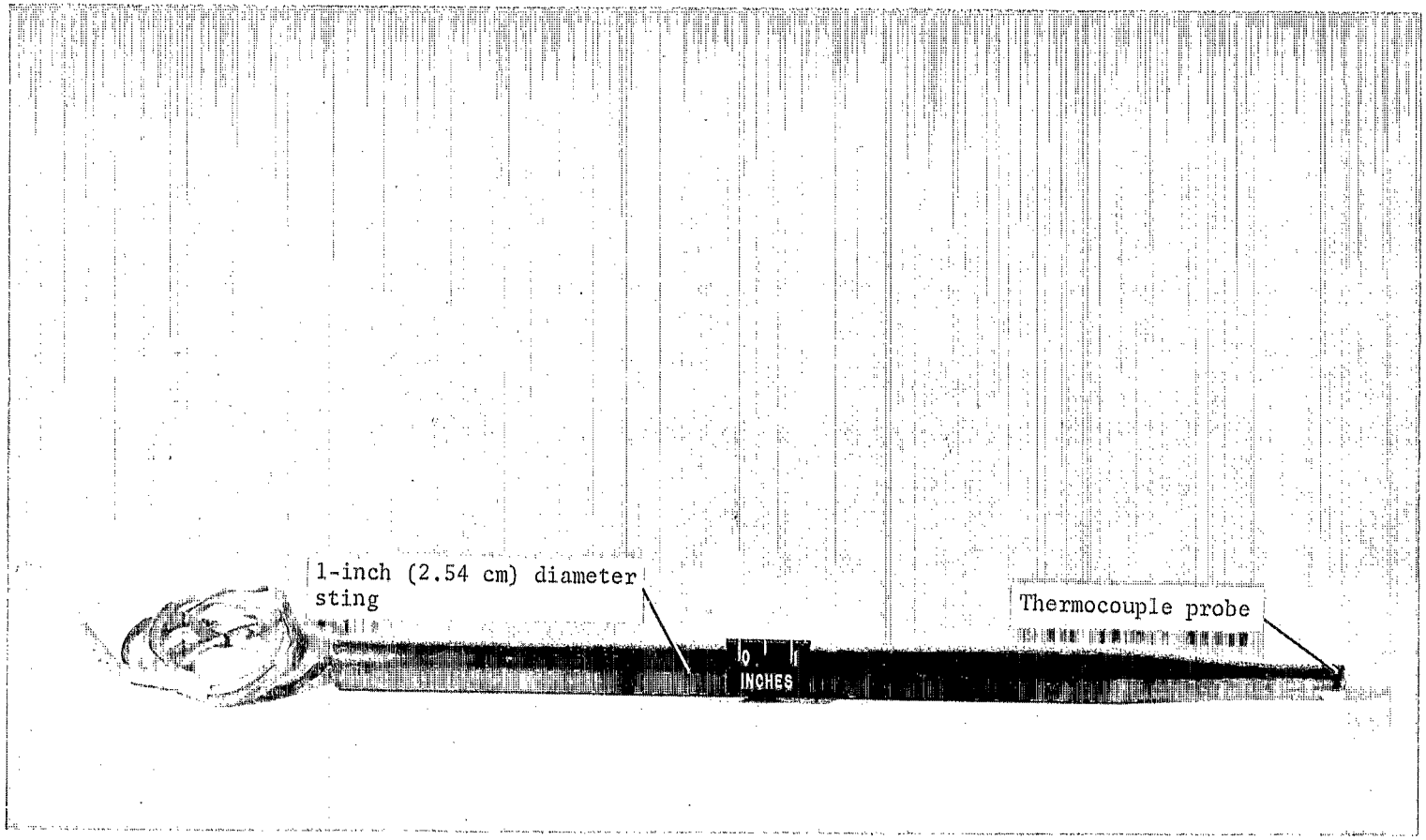


Figure 6.- Photograph of thermocouple probe and support sting. Thermocouple shown is design 7. L-65-3275.1

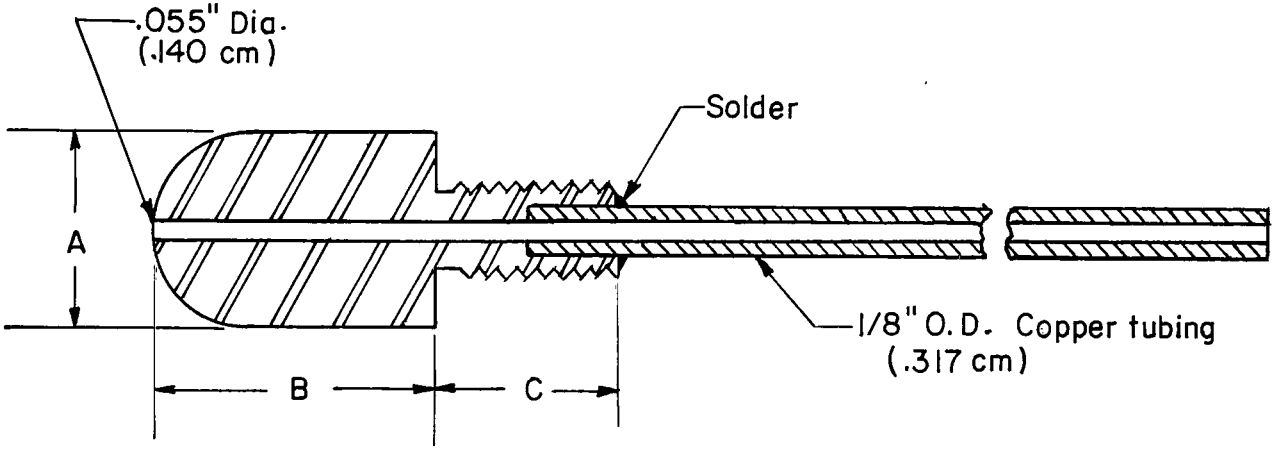


Inches

| A | B | C |
|---|---|---|
| .375 | .750 | .437 |
| .500 | .750 | .500 |
| 1.000 | 1.500 | 1.000 |

Centimeters

| A | B | C |
|---|---|---|
| .953 | 1.905 | 1.110 |
| 1.270 | 1.905 | 1.270 |
| 2.540 | 3.810 | 2.540 |

Figure 7.- Details of pressure probes. Probes have a hemispherical nose.

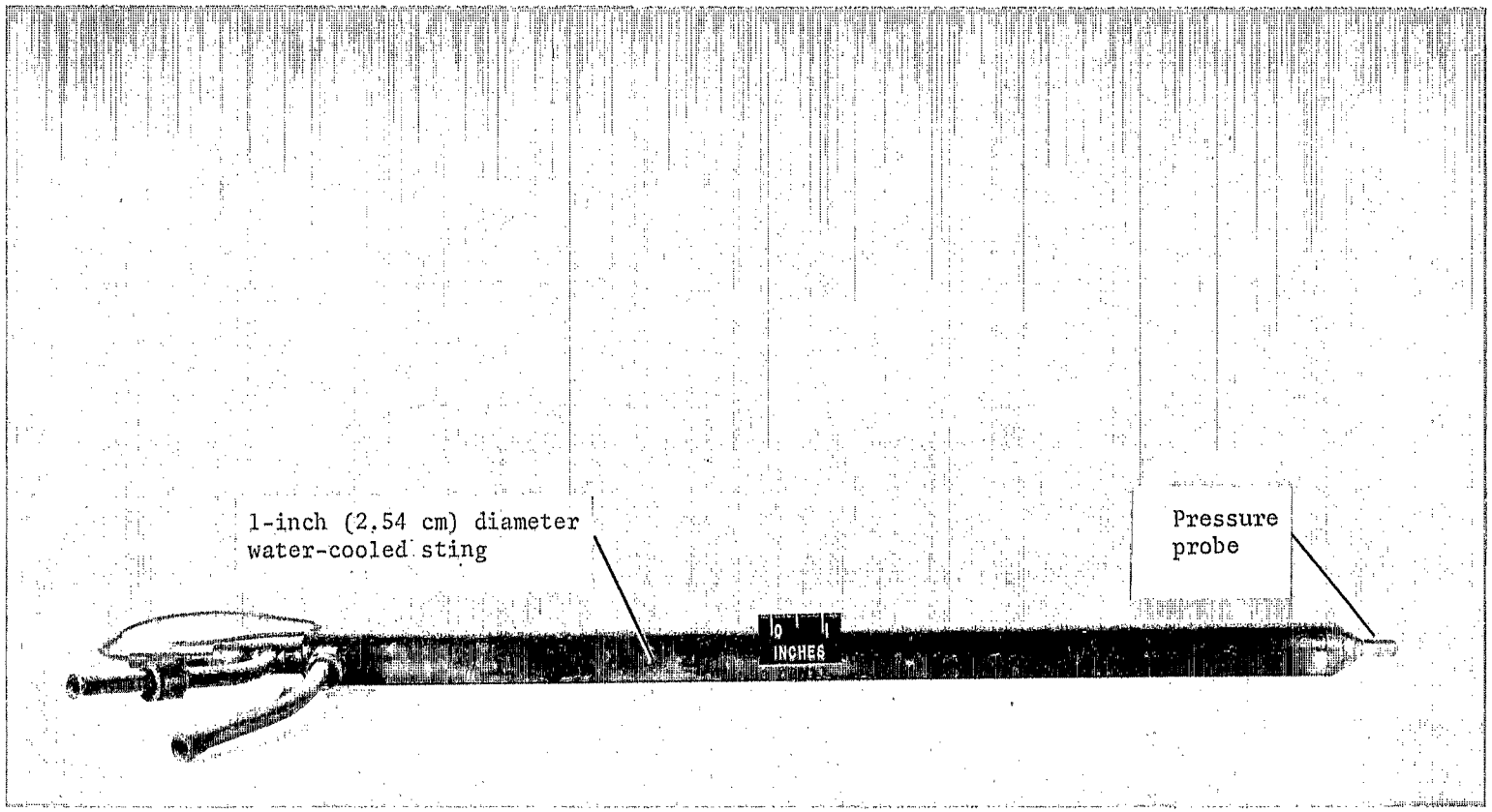


Figure 8.- Photograph of water-cooled support sting with pressure probe. Shown is 0.375-inch (0.953-cm) diameter pressure probe. L-65-3277

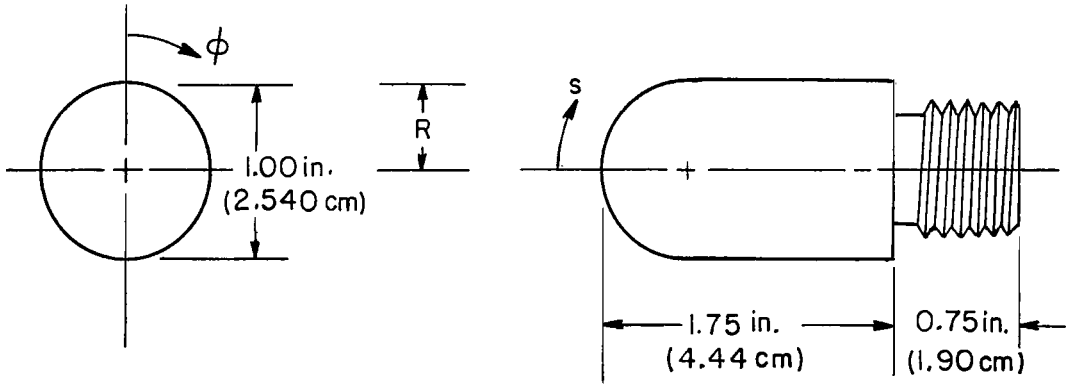


Orifice locations

| s/R | ϕ, deg |
|---|---|
| .00 | — |
| .52 | 0 |
| 1.05 | 240 |
| 1.57 | 120 |
| 1.95 | 0 |
| 2.32 | 0 |

(a) Hemispherical-nose model.

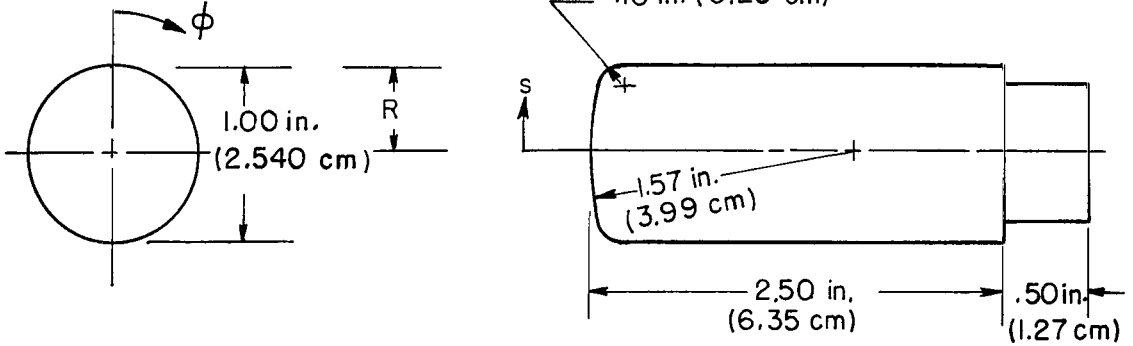


Orifice locations

| s/R | ϕ, deg |
|---|---|
| .00 | — |
| .44 | 0 |
| .44 | 180 |
| .86 | 0 |
| .86 | 180 |
| .97 | 60 |
| .97 | 240 |
| 1.12 | 120 |
| 1.12 | 300 |
| 2.31 | 0 |
| 2.31 | 180 |
| 3.81 | 0 |
| 3.81 | 180 |

(b) Blunt-nose model.

Figure 9.- Exterior sketch of pressure distribution models and their pressure orifice locations.

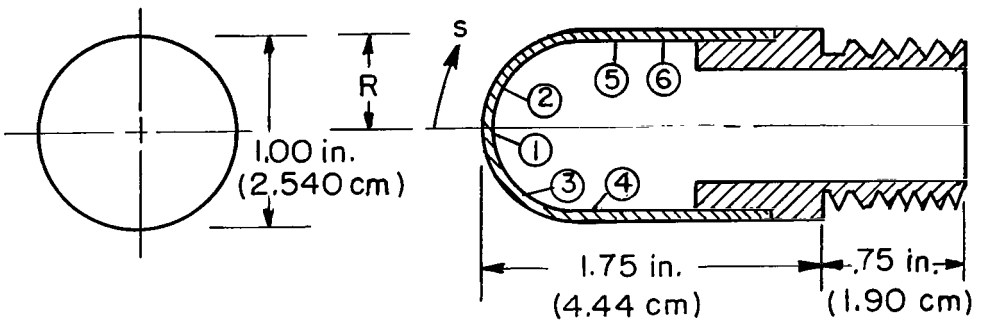


| Thermocouple number | s/R locations |
|---|---|
| 1 | .00 |
| 2 | .52 |
| 3 | 1.05 |
| 4 | 1.57 |
| 5 | 1.95 |
| 6 | 2.32 |

Model 1 – Wall thickness .025 in. (.064 cm)
stagnation-point thermocouple only

Model 2 – Wall thickness .074 in. (.188 cm)
six (6) thermocouple locations

Figure 10.- Sketch of thin-wall models with slope-type calorimeters.

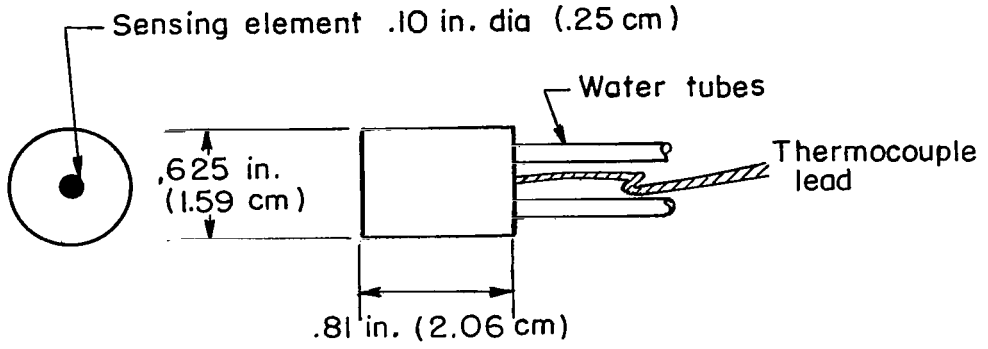


(a) Flat face.

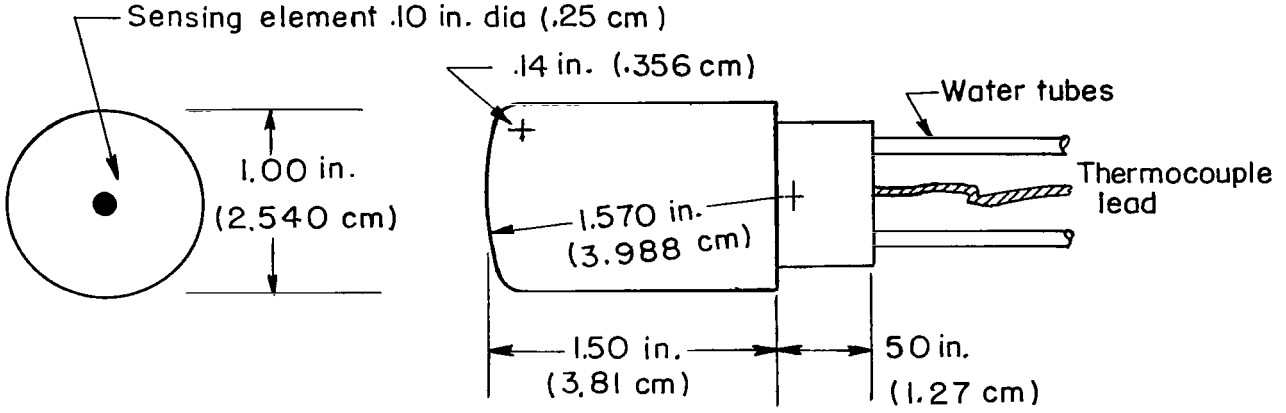


(b) Blunt nose.

Figure 11.- Sketch of models with continuous reading calorimeters.

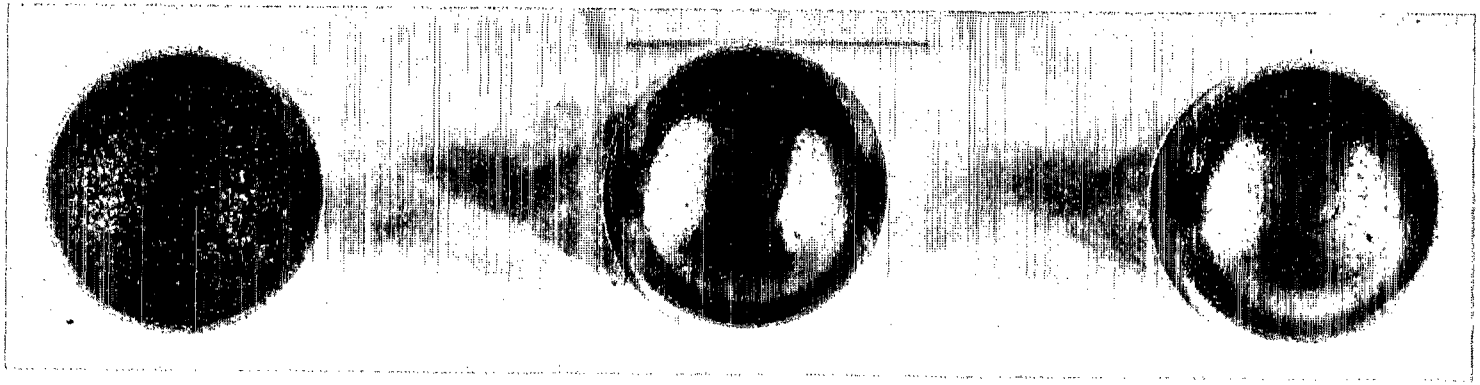

1-inch nozzle (2.5 cm)

3/4-inch nozzle (1.9 cm)

1/2-inch nozzle (1.3 cm)

(a) Exposure time, 30 seconds.

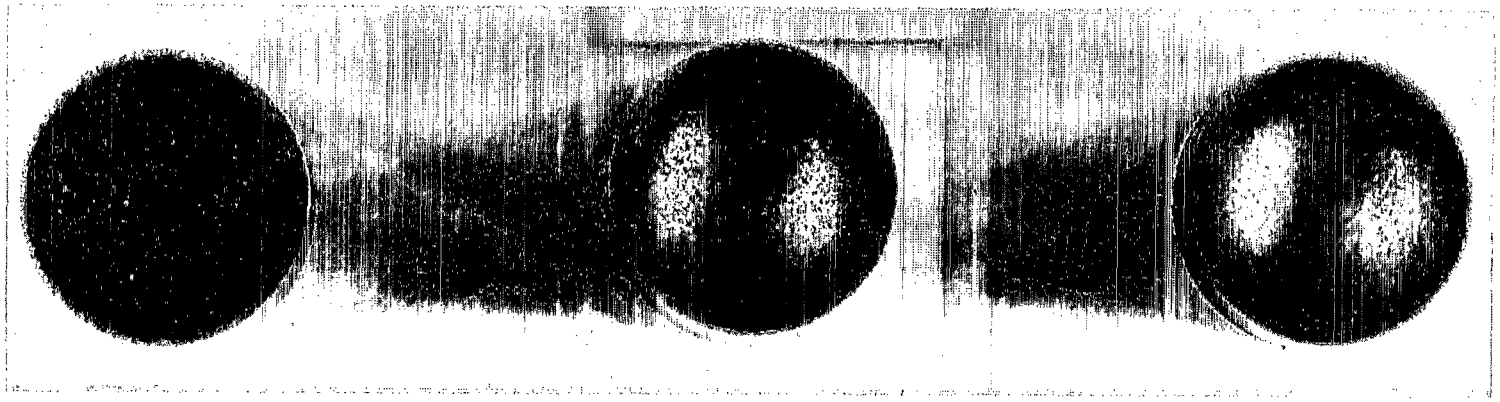

1-inch nozzle (2.5 cm)

3/4-inch nozzle (1.9 cm)

1/2-inch nozzle (1.3 cm)

(b) Exposure time, 240 seconds.

L-68-5609

Figure 12.- Comparison of damage to graphite models in three nozzles of Mach 2 system. Measurements made before a bed cleaning with a cold bed at a chamber pressure of 115 psia (0.79 $MN/m^2$). Models are 0.500-inch (1.270-cm) diameter hemispheres.

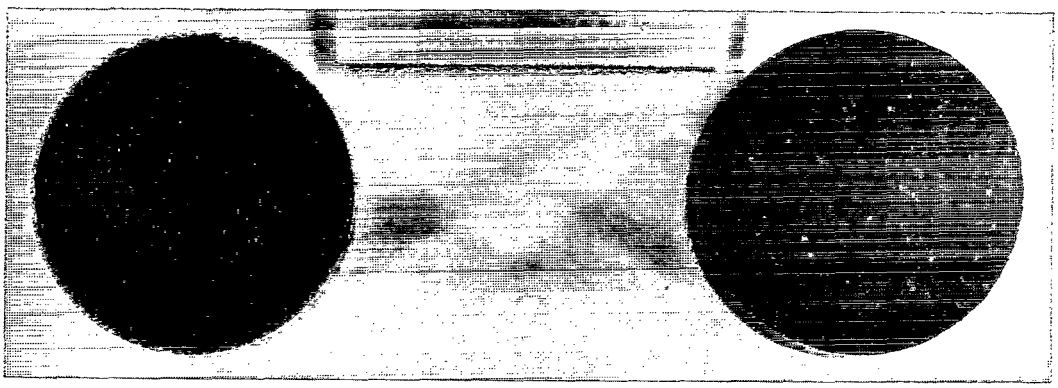

Mach 2 nozzle
$P_{t_2}$ = 81 psia (.56 $MN/m^2$)
weight loss = .0069 grams

Mach 4 nozzle
$P_{t_2}$ = 119 psia (.82 $MN/m^2$)
weight loss = .3148 grams

L-68-5610

Figure 13.- Comparison of damage to graphite models in Mach 2 and Mach 4 nozzles. Exposure time of 30 seconds. Models are 0.500-inch (1.270-cm) diameter hemispheres.

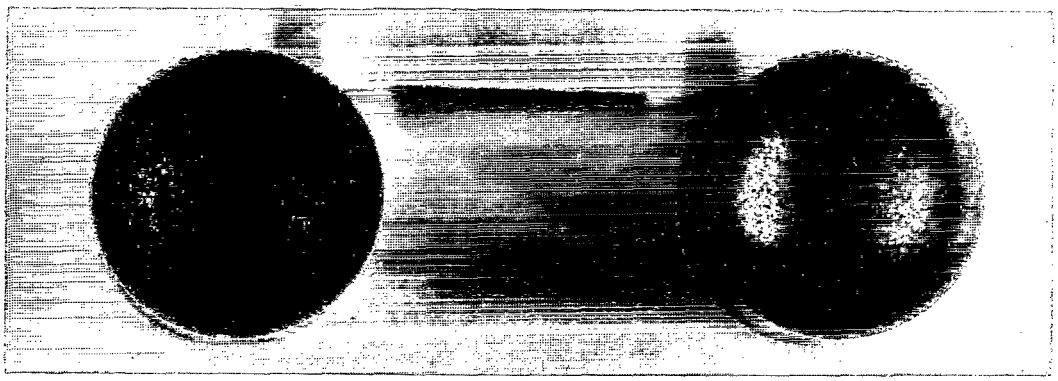

Before

After

L-68-5611

Figure 14.- Effect of bed cleaning on damage to a graphite model in 1-inch (2.5-cm) nozzle of Mach 2 system. Exposure time, 30 seconds; chamber pressure, 115 psia (0.79 $MN/m^2$). Models are 0.500-inch (1.270-cm) diameter hemispheres.

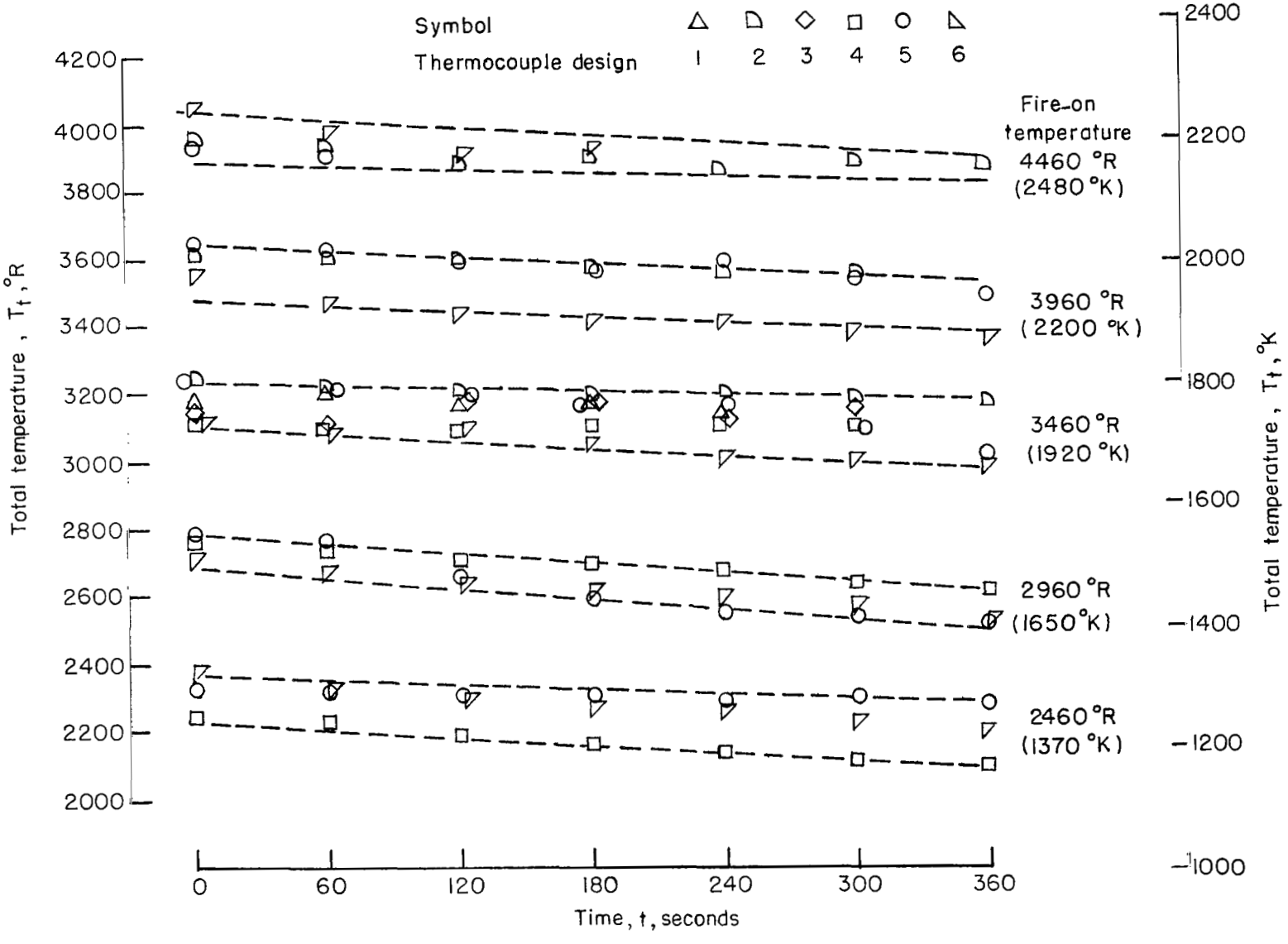


Figure 15.- Total temperature history. Data taken in 1-inch (2.5-cm) nozzle at a chamber pressure of 115 psia (0.79 MN/m$^2$). Measurements taken 0.25 inch (0.62 cm) from exit plane of nozzle.

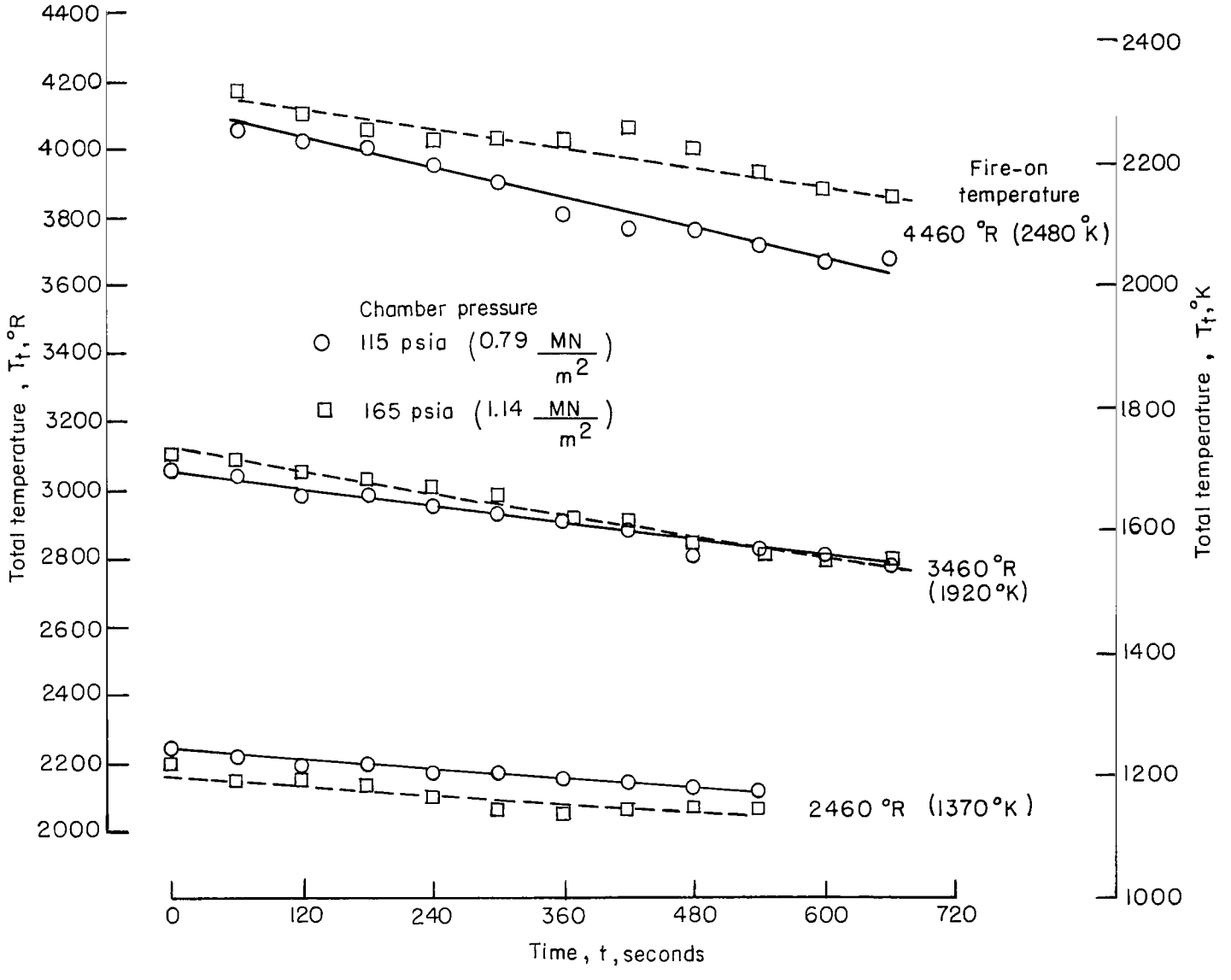


Figure 16.- Effect of chamber pressure on total temperature history. Measurements were taken in 1-inch (2.5-cm) nozzle at 0.50 inch (1.27 cm) from exit plane of nozzle using thermocouple design 7.

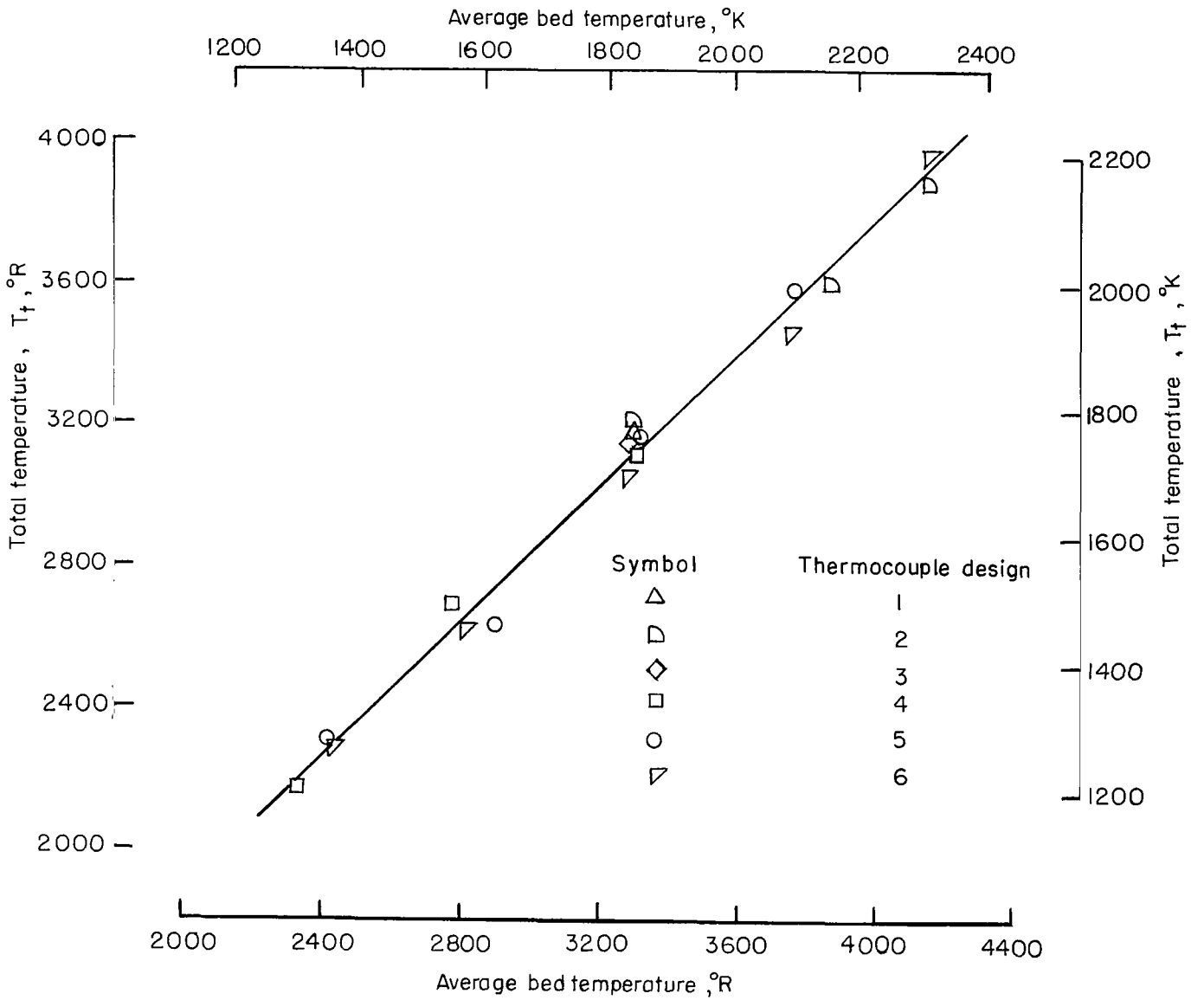


Figure 17.- Correlation between average bed temperature at surface of pebbles and total temperature of airstream. Total temperature is an average total temperature based on test times of approximately 360 seconds. Data taken in the 1-inch (2.5-cm) nozzle at a chamber pressure of 115 psia (0.79 MN/m2).

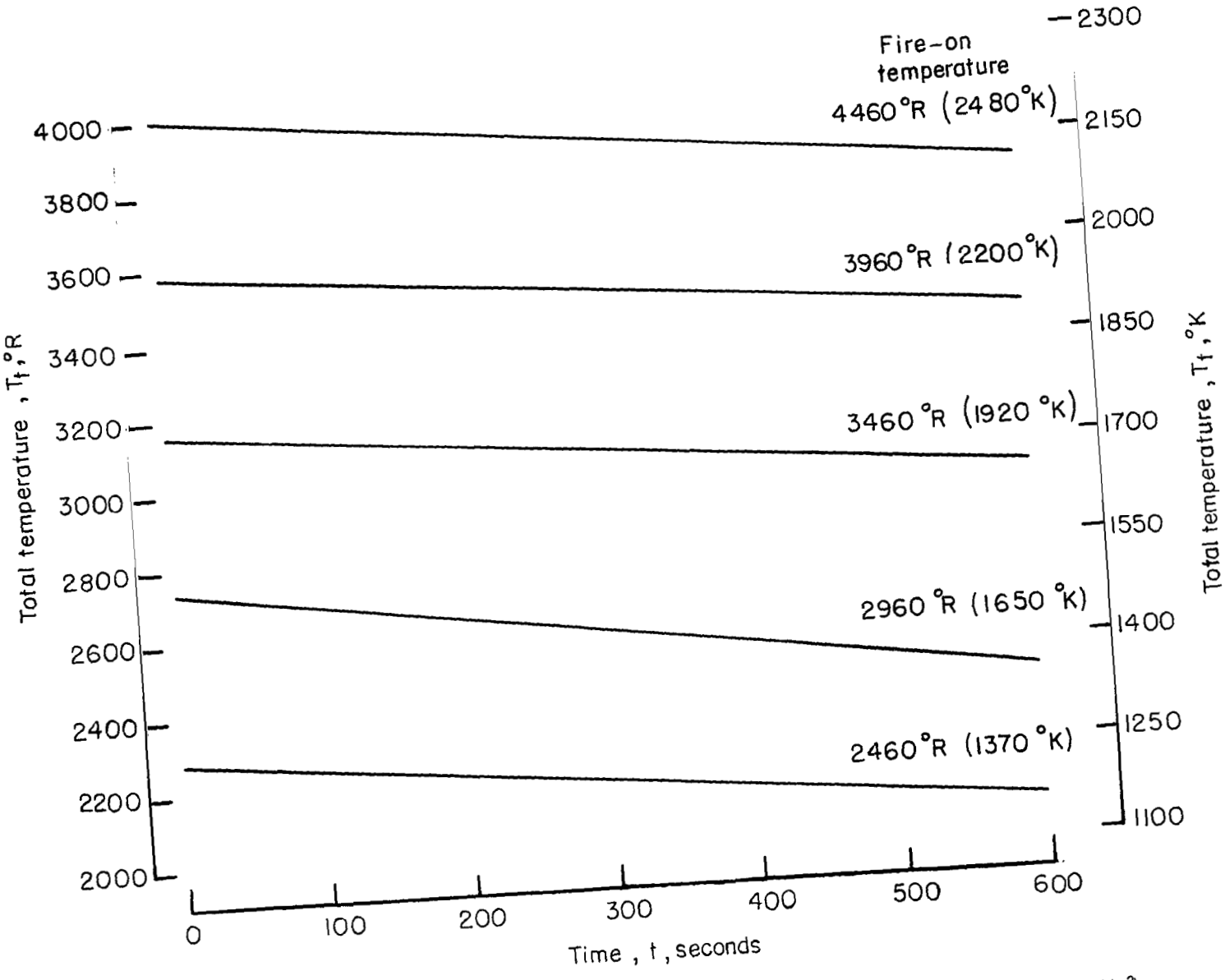


Figure 18.- Average total temperature decay in 1-inch (2.5-cm) nozzle. Chamber pressure in range 115 to 165 psia (0.79 to 1.14 MN/m2). Time zero is based on 180 to 240 seconds from fire on until test begins.

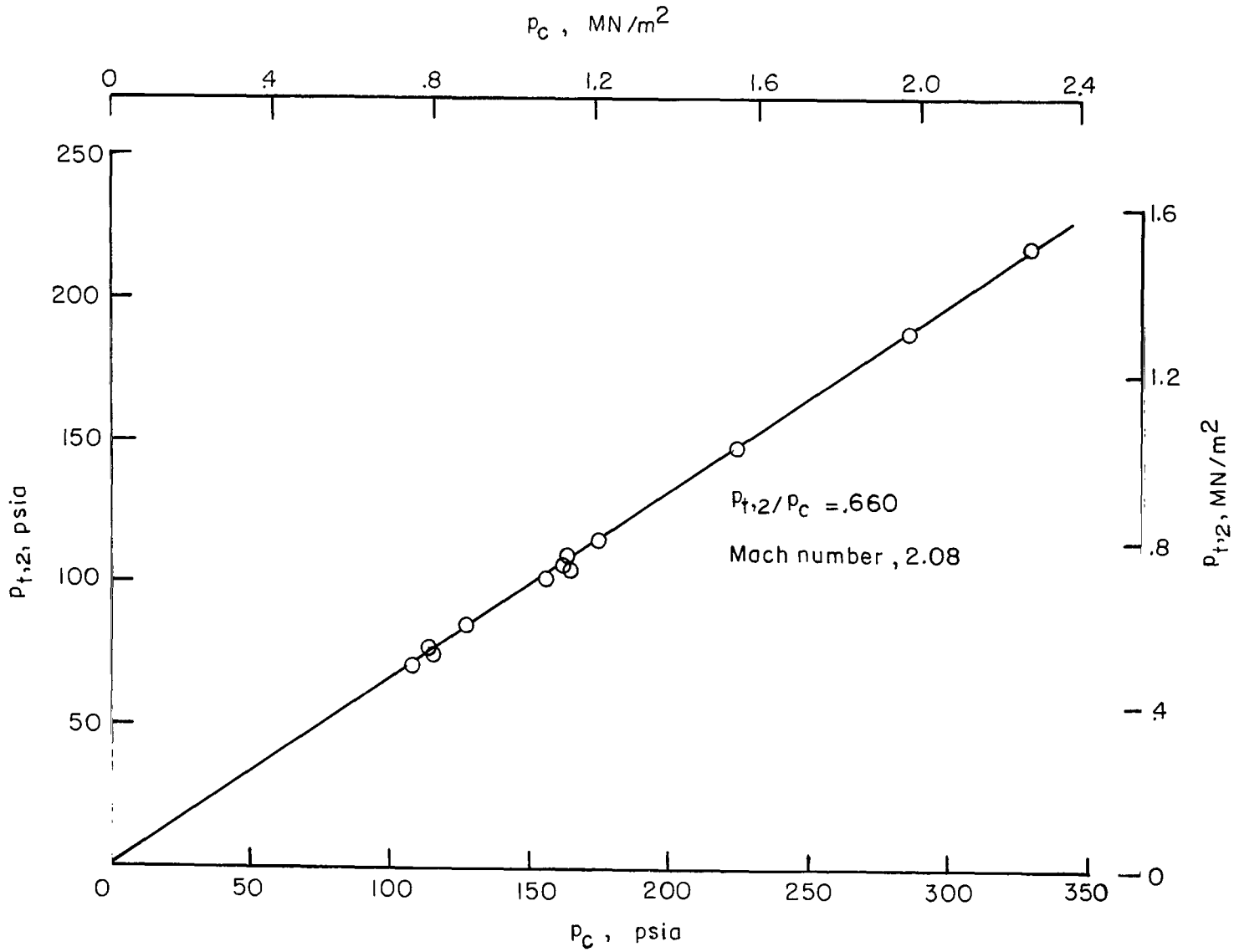


Figure 19.- Correlation of the total pressures across shock wave for 1-inch (2.5-cm) nozzle at a distance of 0.50 inch (1.27 cm) from exit plane of nozzle. Total temperature, 3950° R (2200° K).

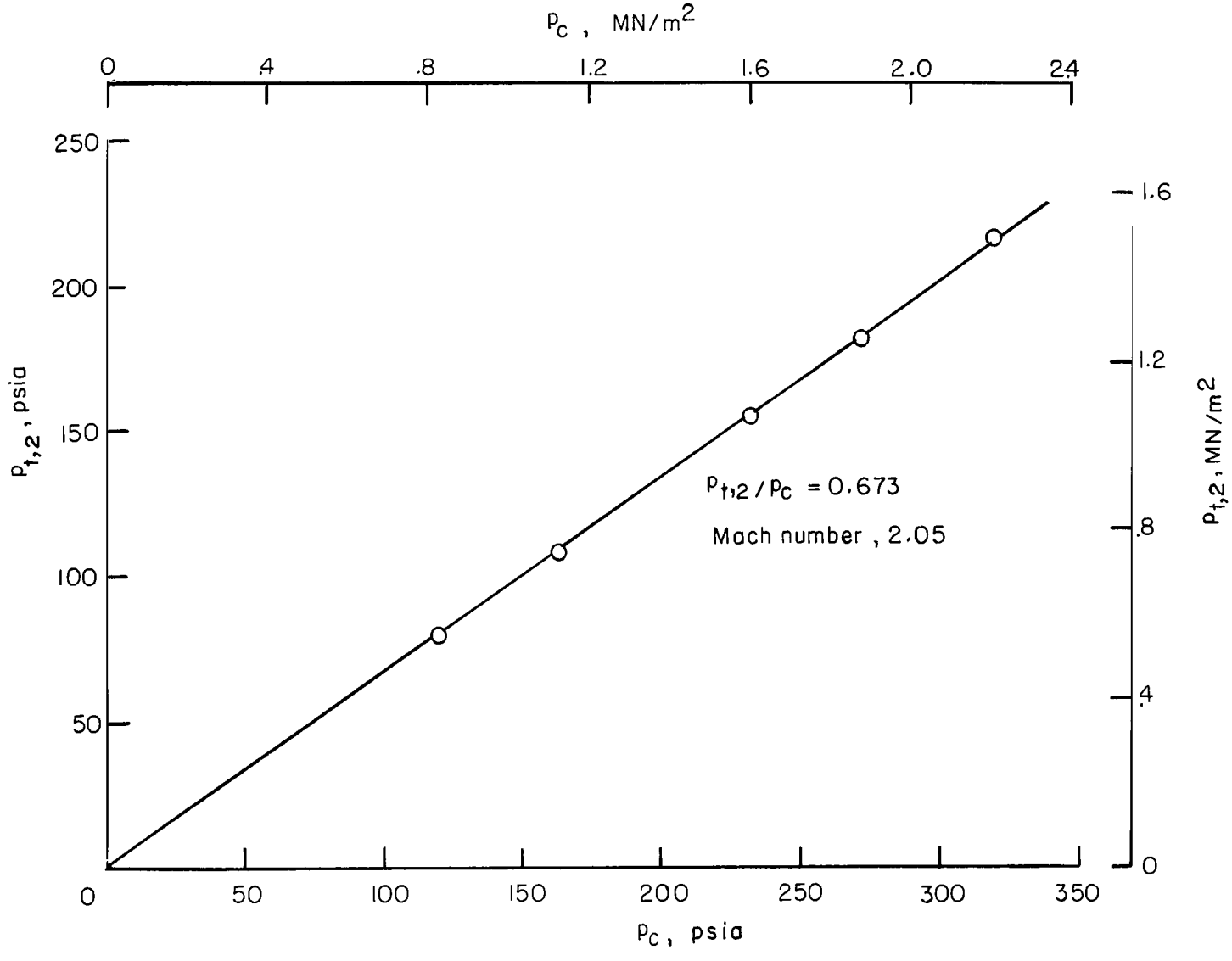


Figure 20.- Correlation of total pressures across shock wave for 3/4-inch (1.9-cm) nozzle at a distance of 0.50 inch (1.27 cm) from exit plane of nozzle. Total temperature, 3950° R (2200° K).

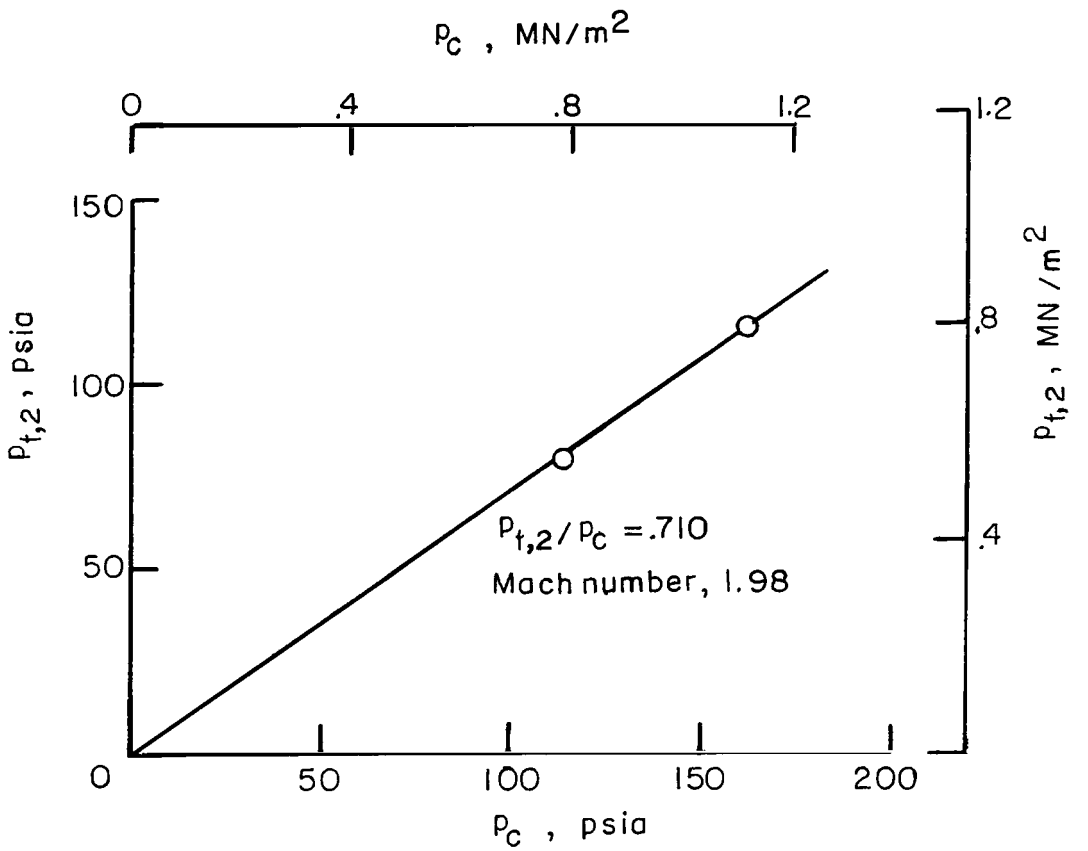


Figure 21.- Correlation of total pressures across the shock wave for 1/2-inch (1.3-cm) nozzle at a distance of 0.12 inch (0.32 cm) from exit plane of nozzle. Total temperature, $3950^0$ R ($2200^0$ K).

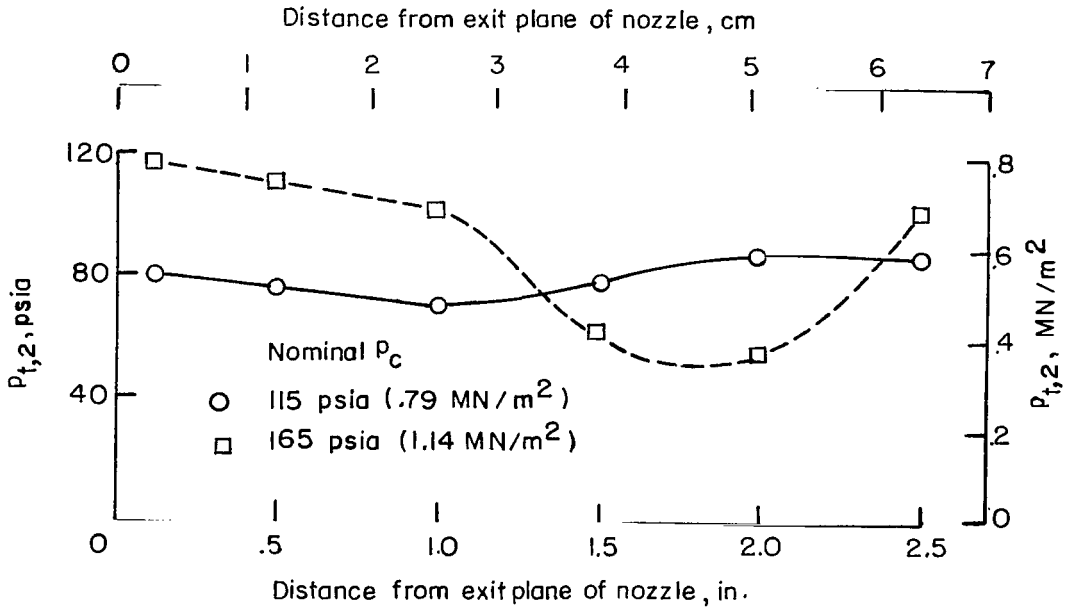


(a) Total pressure behind shock wave.

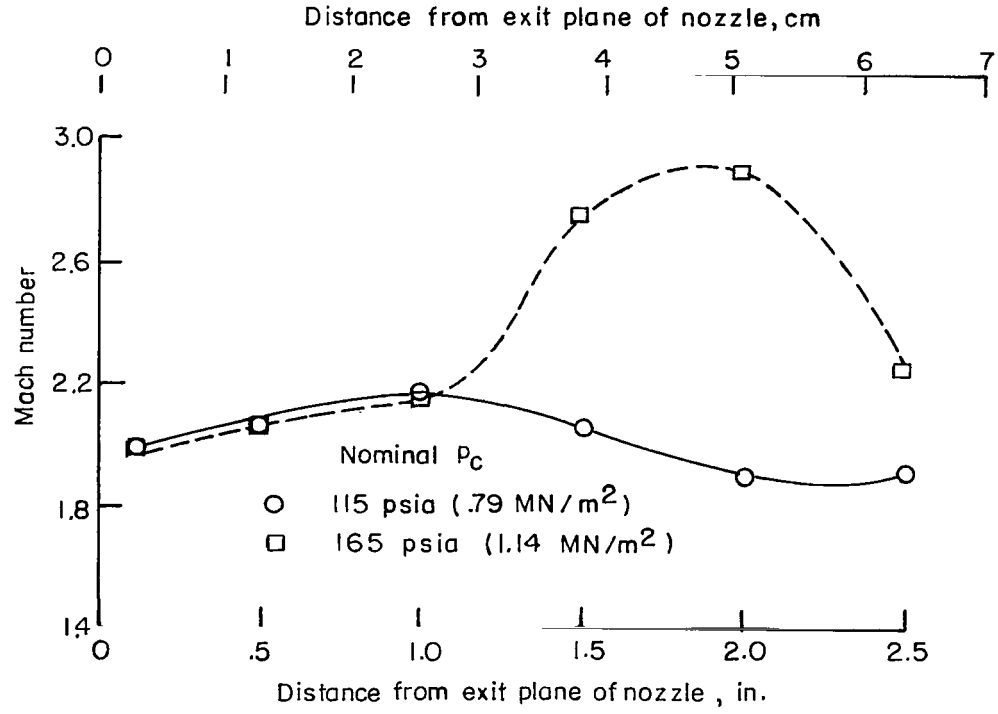


(b) Mach number.

Figure 22.- Variation of total pressure behind shock wave and local free-stream Mach number with distance from exit plane of 1-inch (2.5-cm) nozzle.

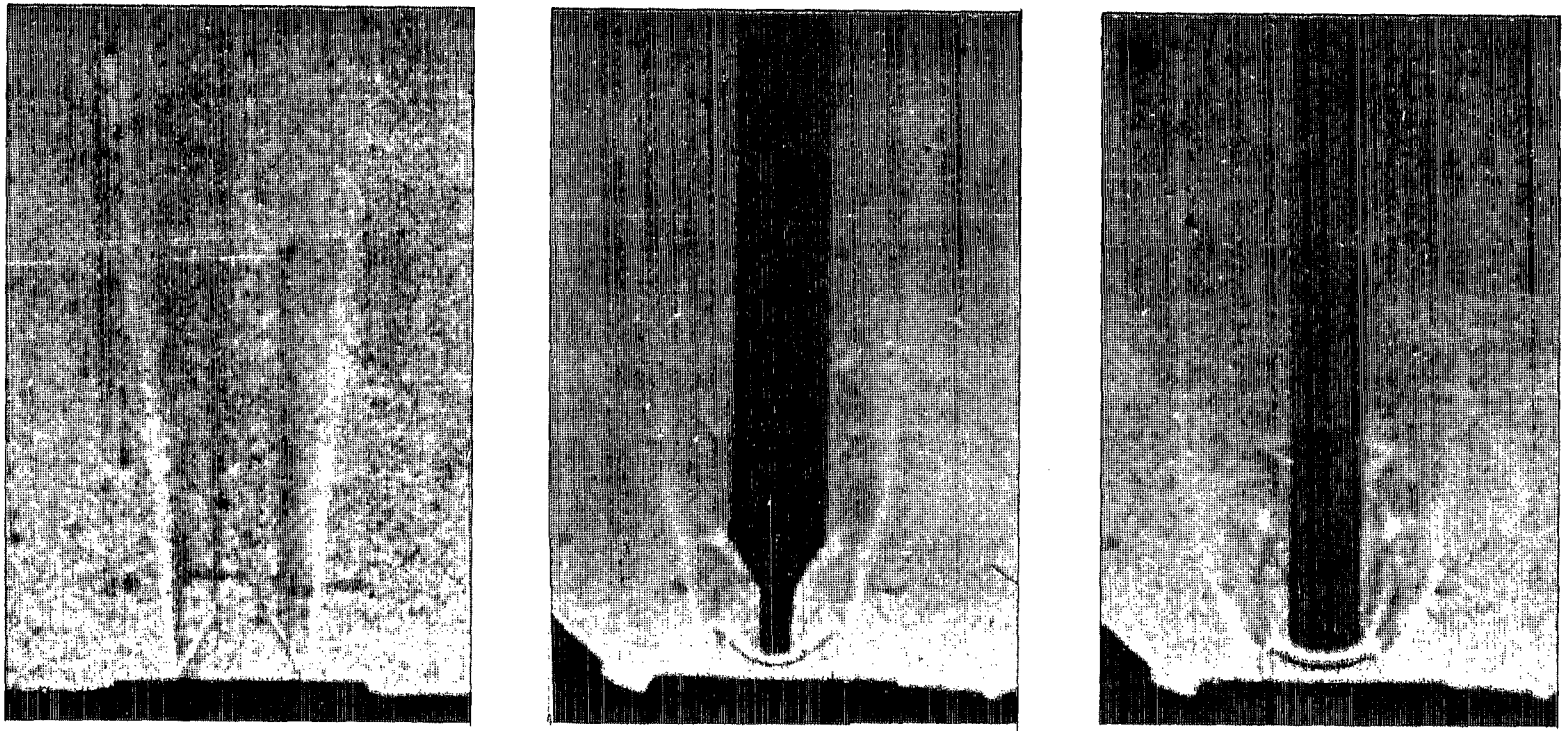

(a) Free stream. (b) 3/8-inch (0.95-cm) diameter model. (c) 3/4-inch (1.90-cm) diameter model.

L-68-5612

Figure 23.- Shadowgraphs of flow field of 1-inch (2.5-cm) nozzle at a chamber pressure of 115 psia (0.79 MN/m2). Models shown in parts (b) and (c) are hemispherical-nose models.

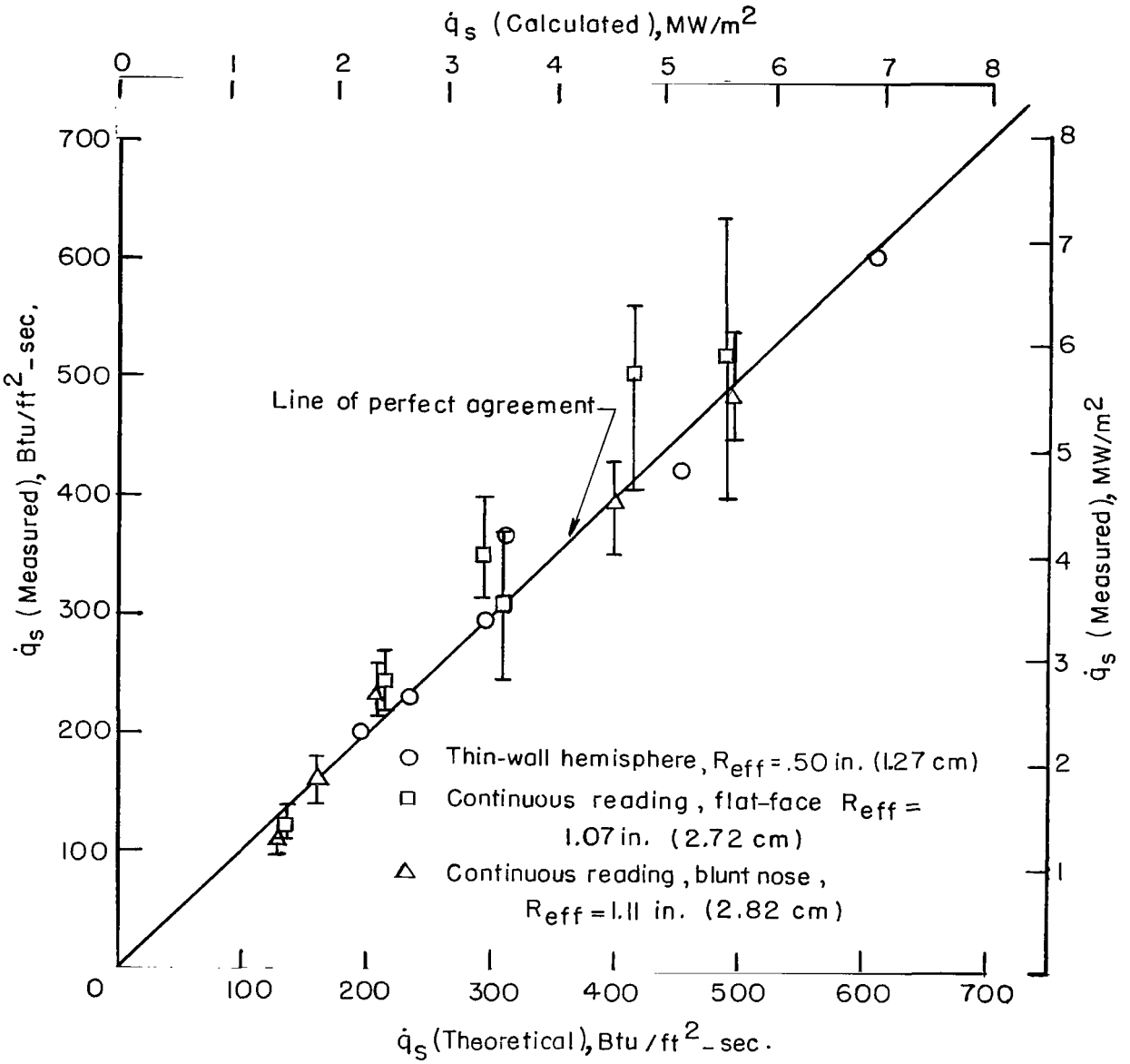


Figure 24.- Comparison between measured and theoretical stagnation-point heating rates in 1-inch (2.5-cm) nozzle.

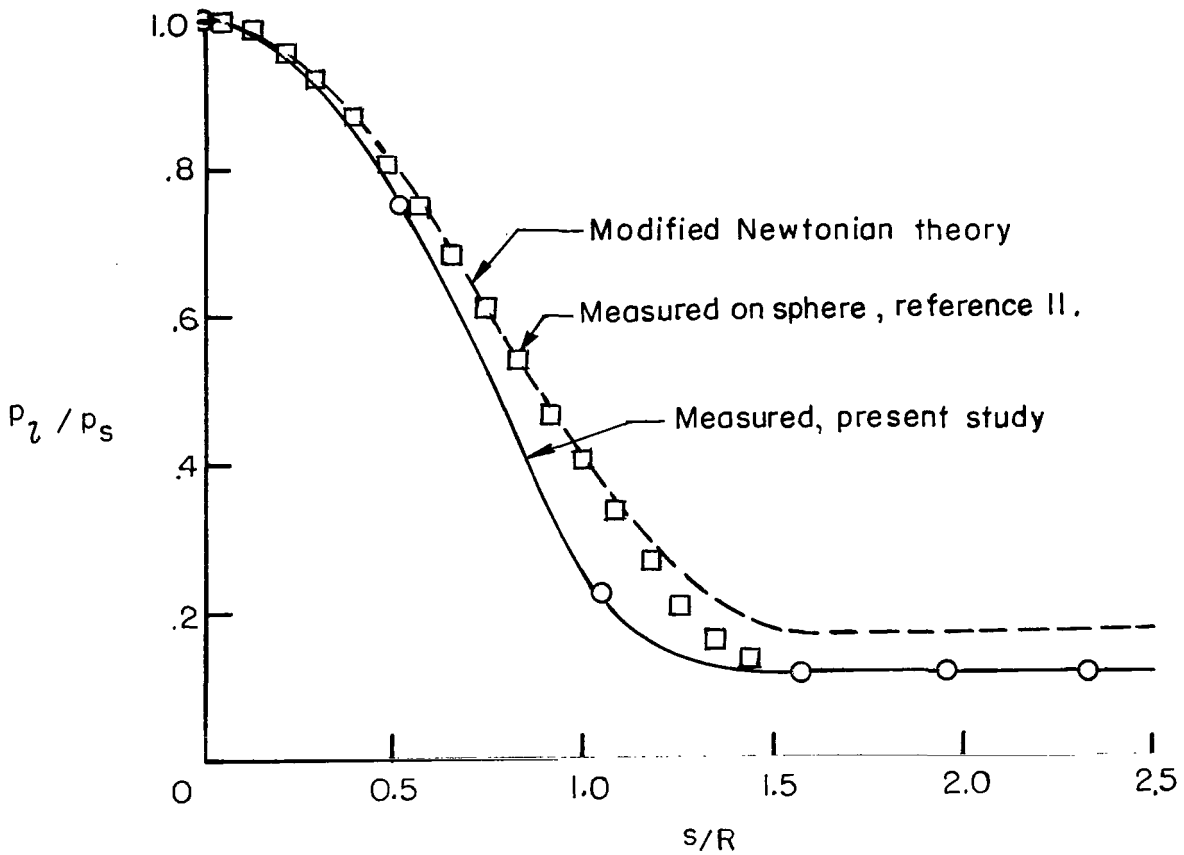


(a) $p_c$ = 133 psia; $p_{t,2}$ = 88 psia; $T_t$ = 4000° R ($p_c$ = 0.91 MN/m$^2$; $p_{t,2}$ = 0.61 MN/m$^2$; $T_t$ = 2220° K).

Figure 25.- Normalized pressure distribution over hemisphere-cylinder model in 1-inch (2.5-cm) nozzle at a distance of 0.50 inch (1.27 cm) from nozzle exit.

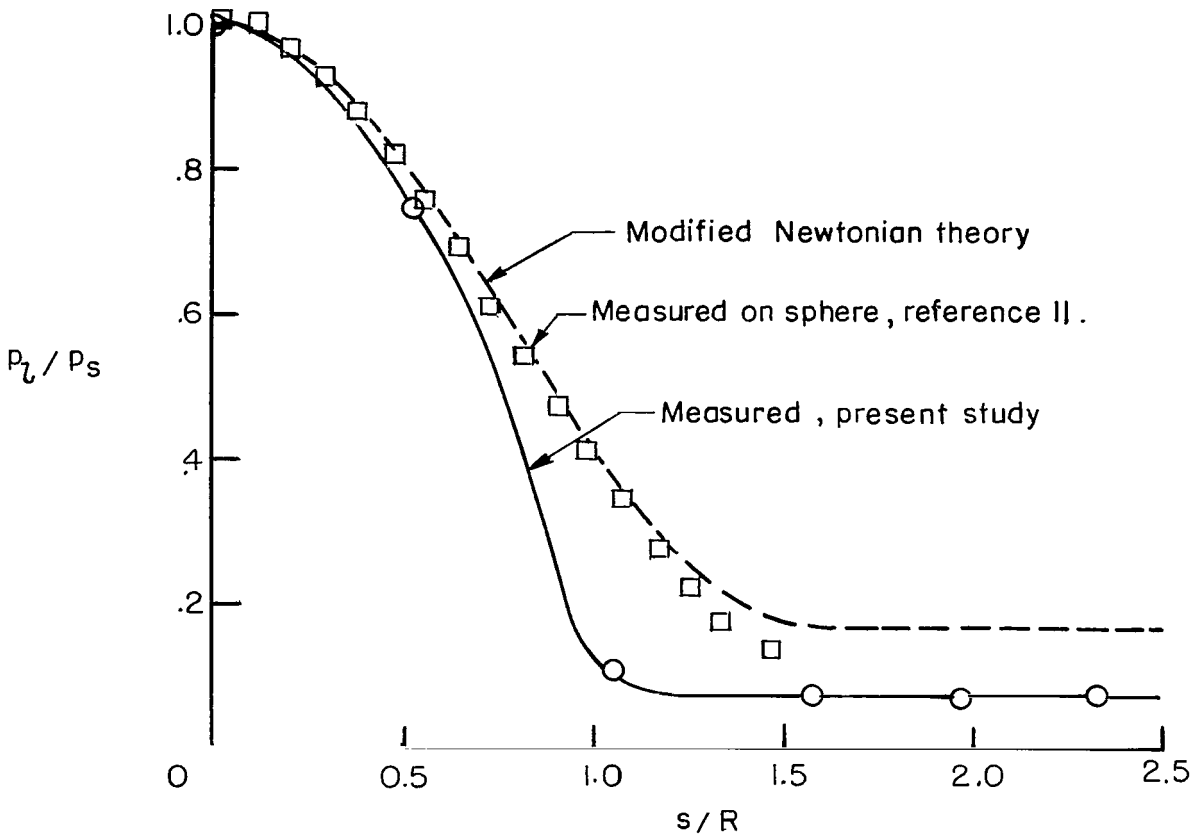


(b) $p_c$ = 241 psia; $p_{t,2}$ = 157 psia; $T_t$ = 4000° R ($p_c$ = 1.66 MN/m$^2$; $p_{t,2}$ = 1.08 MN/m$^2$; $T_t$ = 2220° K).

Figure 25.- Concluded.

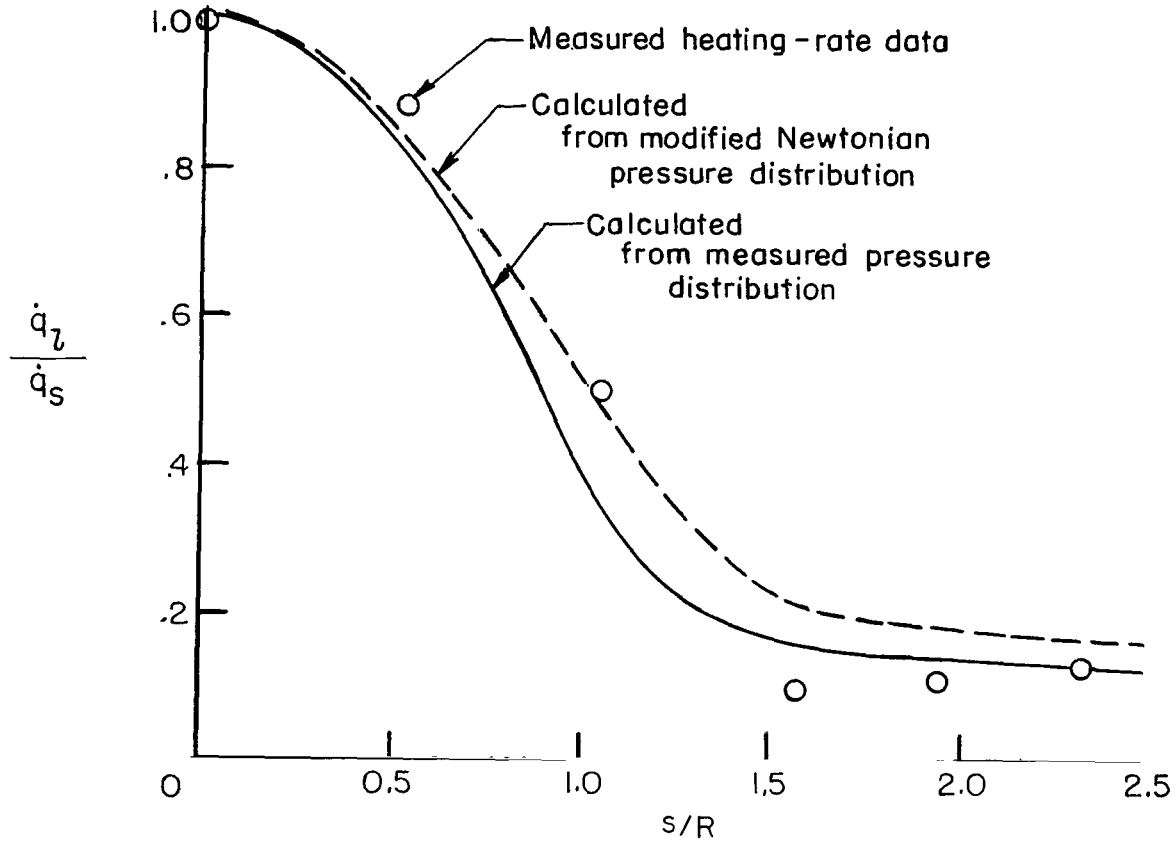


(a) $p_c$ = 133 psia; $p_{t,2}$ = 88 psia; $T_t$ = 4000° R ($p_c$ = 0.91 MN/m$^2$; $p_{t,2}$ = 0.61 MN/m$^2$; $T_t$ = 2220° K).

Figure 26.- Normalized heating-rate distribution over hemisphere-cylinder model in 1-inch (2.5-cm) nozzle at a distance of 0.50 inch (1.27 cm) from nozzle exit.

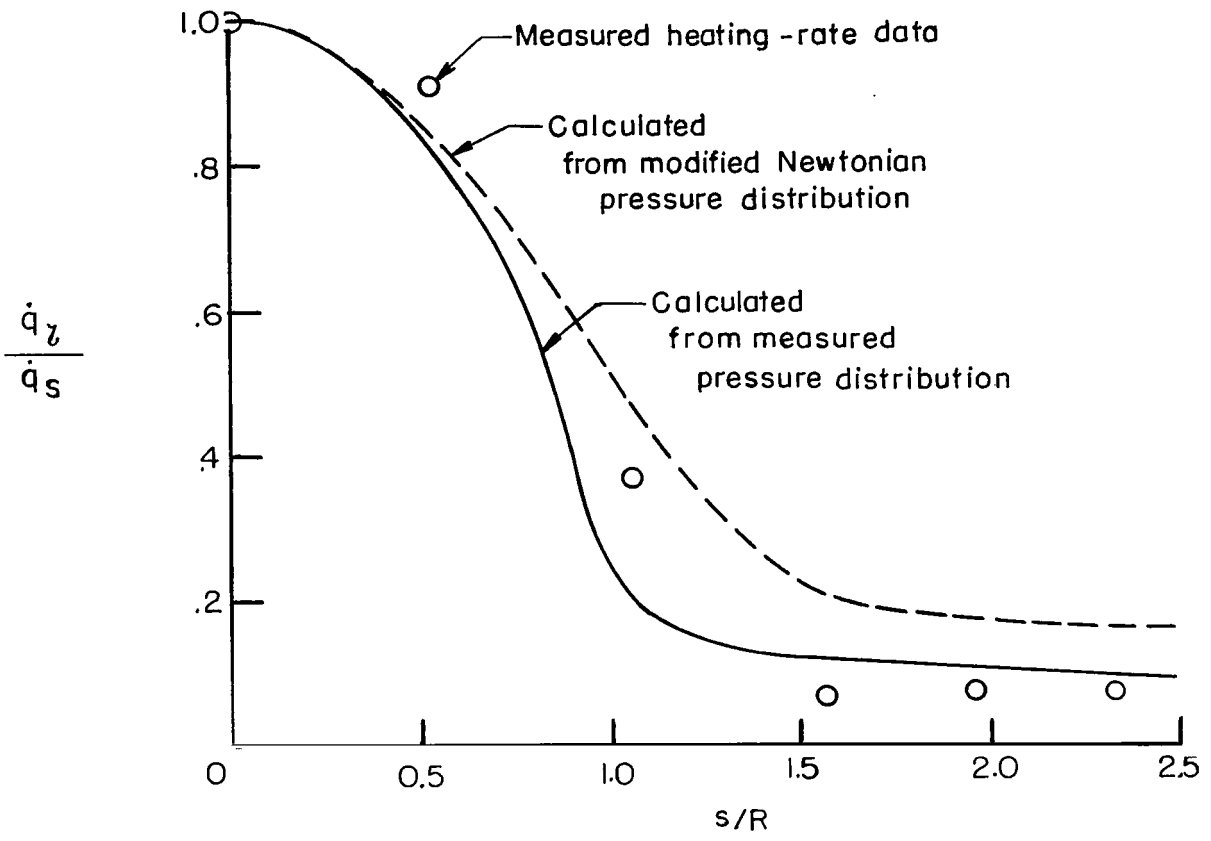


(b) $p_c$ = 241 psia; $p_{t,2}$ = 157 psia; $T_t$ = 4000° R ($p_c$ = 1.66 MN/m$^2$; $p_{t,2}$ = 1.08 MN/m$^2$; $T_t$ = 2220° K).

Figure 26.- Concluded.

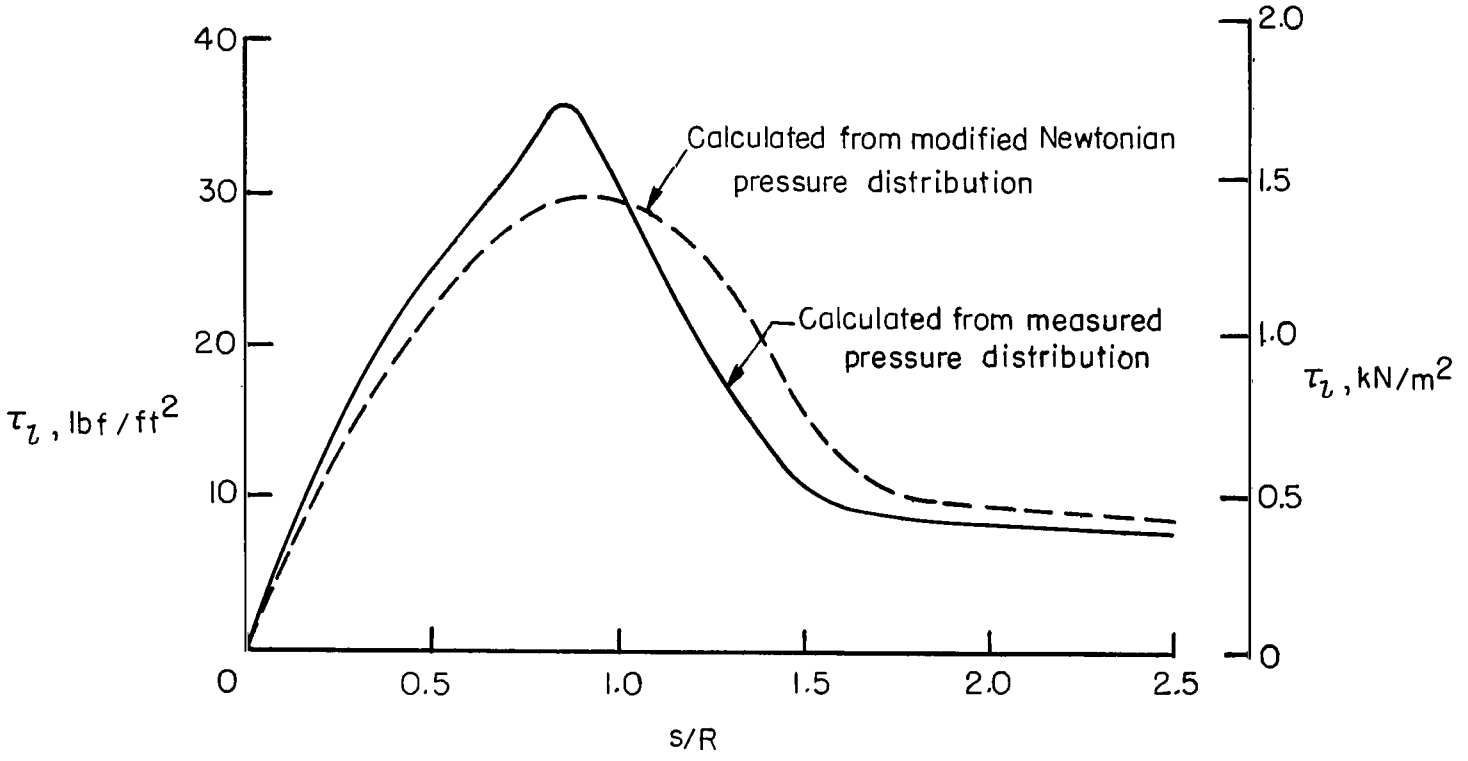


(a) $p_c$ = 133 psia; $p_{t,2}$ = 88 psia; $T_t$ = 4000° R ($p_c$ = 0.91 MN/m$^2$; $p_{t,2}$ = 0.61 MN/m$^2$; $T_t$ = 2220° K).

Figure 27.- Calculated aerodynamic shear distribution over hemisphere-cylinder model in 1-inch (2.5-cm) nozzle.

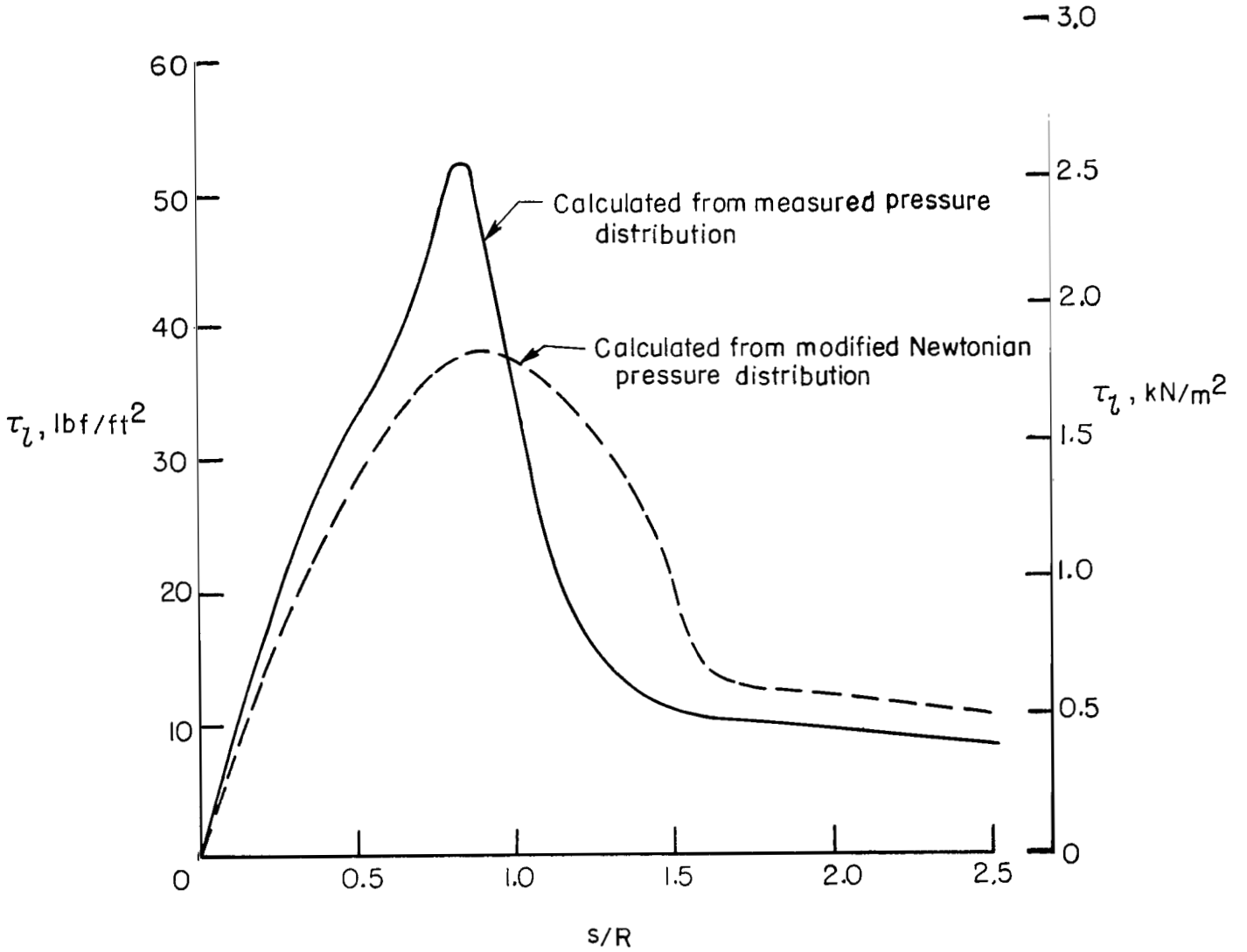


(b) $p_c$ = 241 psia; $p_{t,2}$ = 157 psia; $T_t$ = 4000° R ($p_c$ = 1.66 MN/m$^2$; $p_{t,2}$ = 1.08 MN/m$^2$; $T_t$ = 2220° K).

Figure 27.- Concluded.

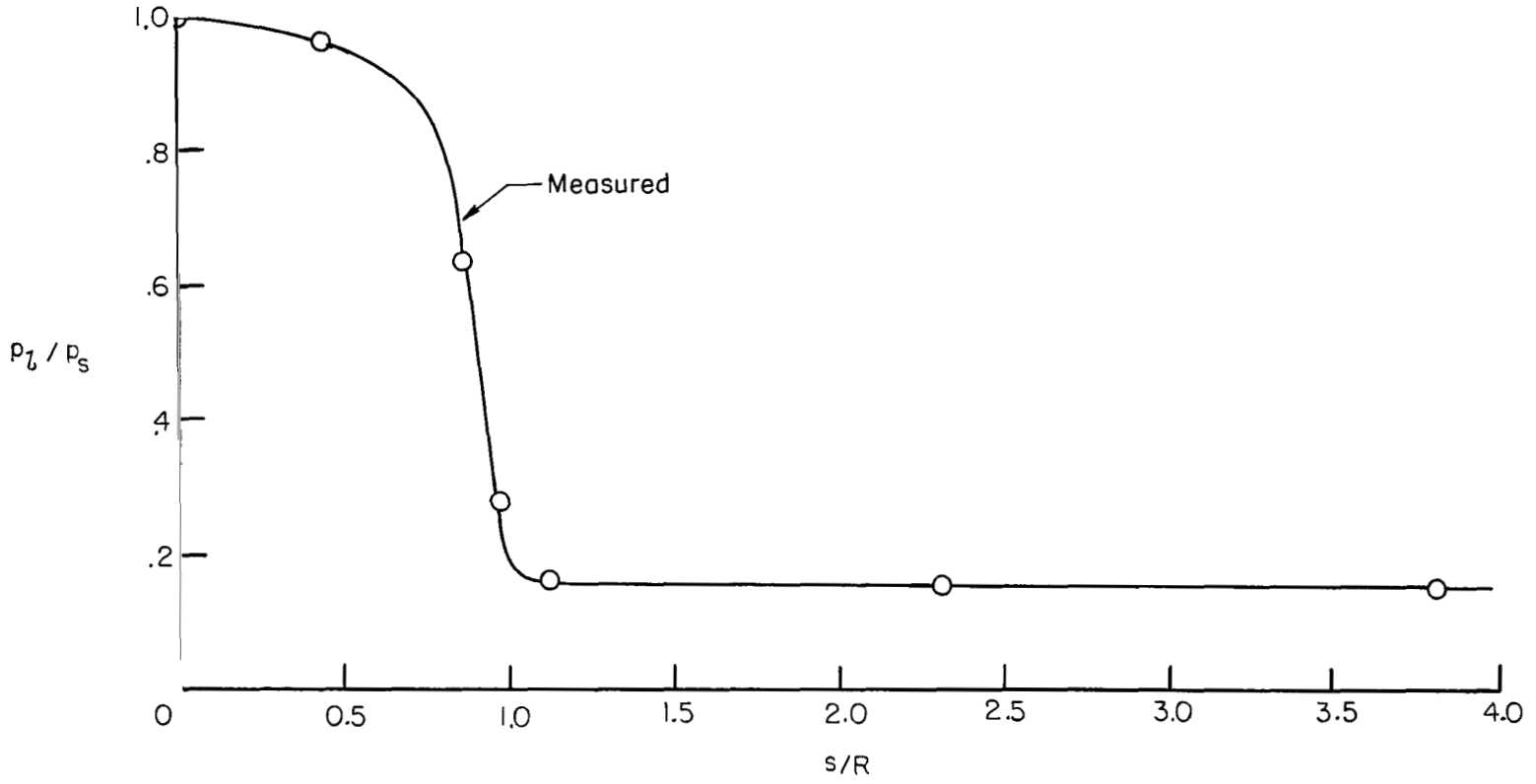


(a) $p_c$ = 121 psia; $p_{t,2}$ = 84 psia; $T_t$ = 2160° R $\left(p_c = 0.83\ MN/m^2;\ p_{t,2} = 0.56\ MN/m^2;\ T_t = 1200°\ K\right)$.

Figure 28.- Normalized measured pressure distribution over blunt-nose cylinder model in 1-inch (2.5-cm) nozzle at a distance of 0.50 inch (1.27 cm) from nozzle exit.

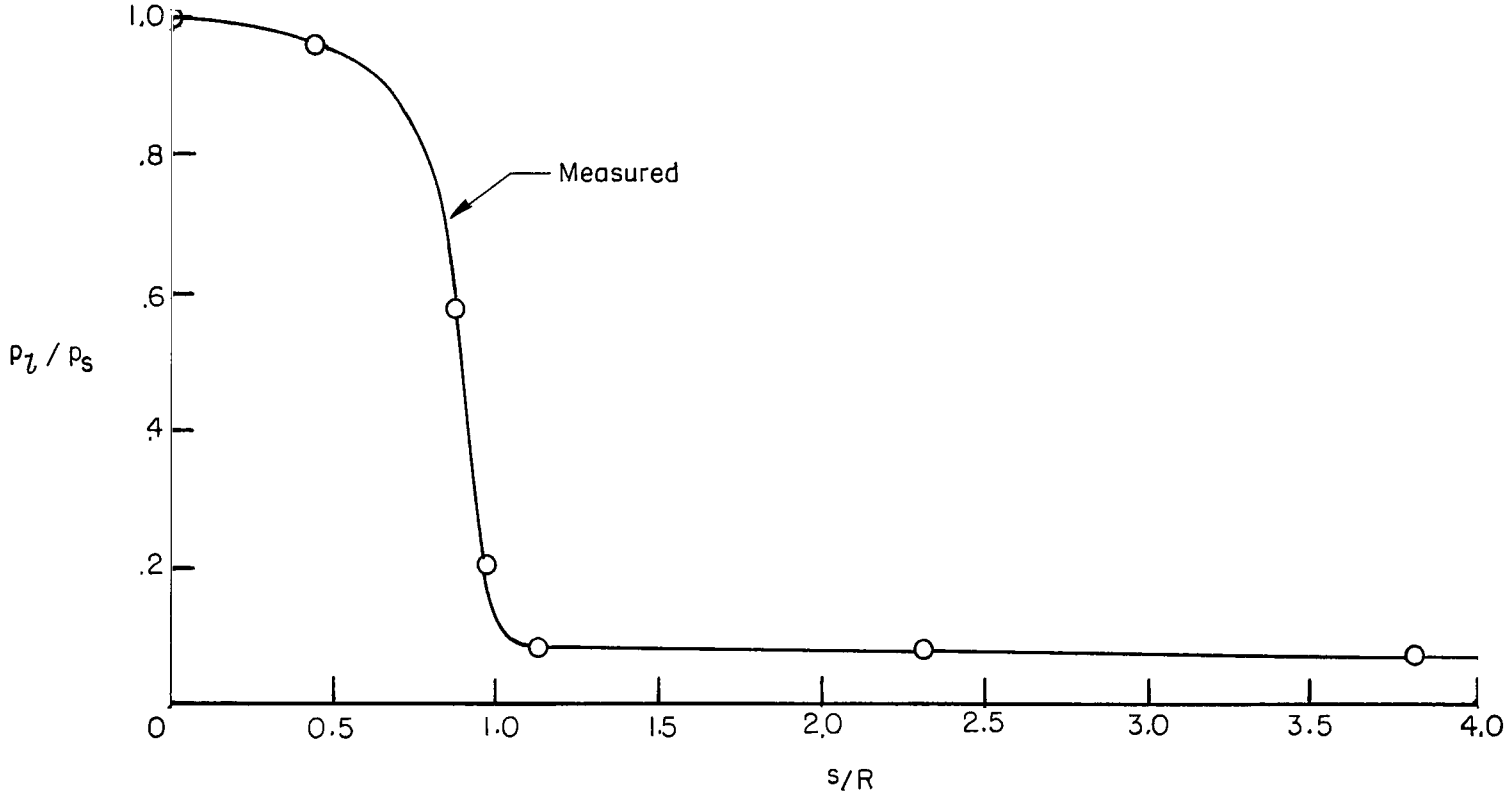


(b) $p_c$ = 232 psia; $p_{t,2}$ = 154 psia; $T_t$ = 4000° R ($p_c$ = 1.60 MN/m$^2$; $p_{t,2}$ = 1.06 MN/m$^2$; $T_t$ = 2220° K).

Figure 28.- Concluded.

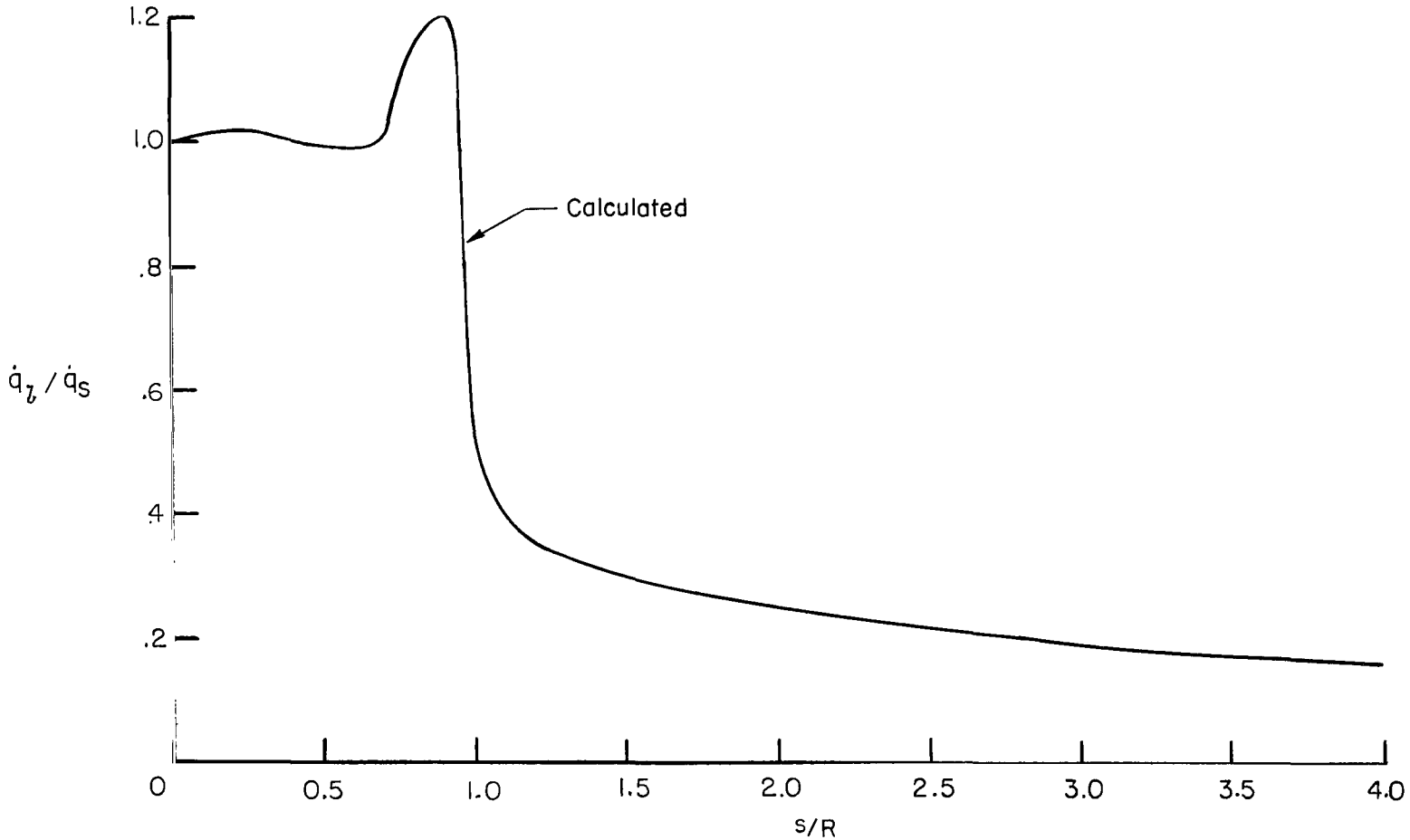


(a) $p_c$ = 121 psia; $p_{t,2}$ = 84 psia; $T_t$ = 2160° R ($p_c$ = 0.83 MN/m$^2$; $p_{t,2}$ = 0.56 MN/m$^2$; $T_t$ = 1200° K).

Figure 29.- Normalized calculated heating-rate distribution over blunt-nose cylinder model in 1-inch (2.5-cm) nozzle.

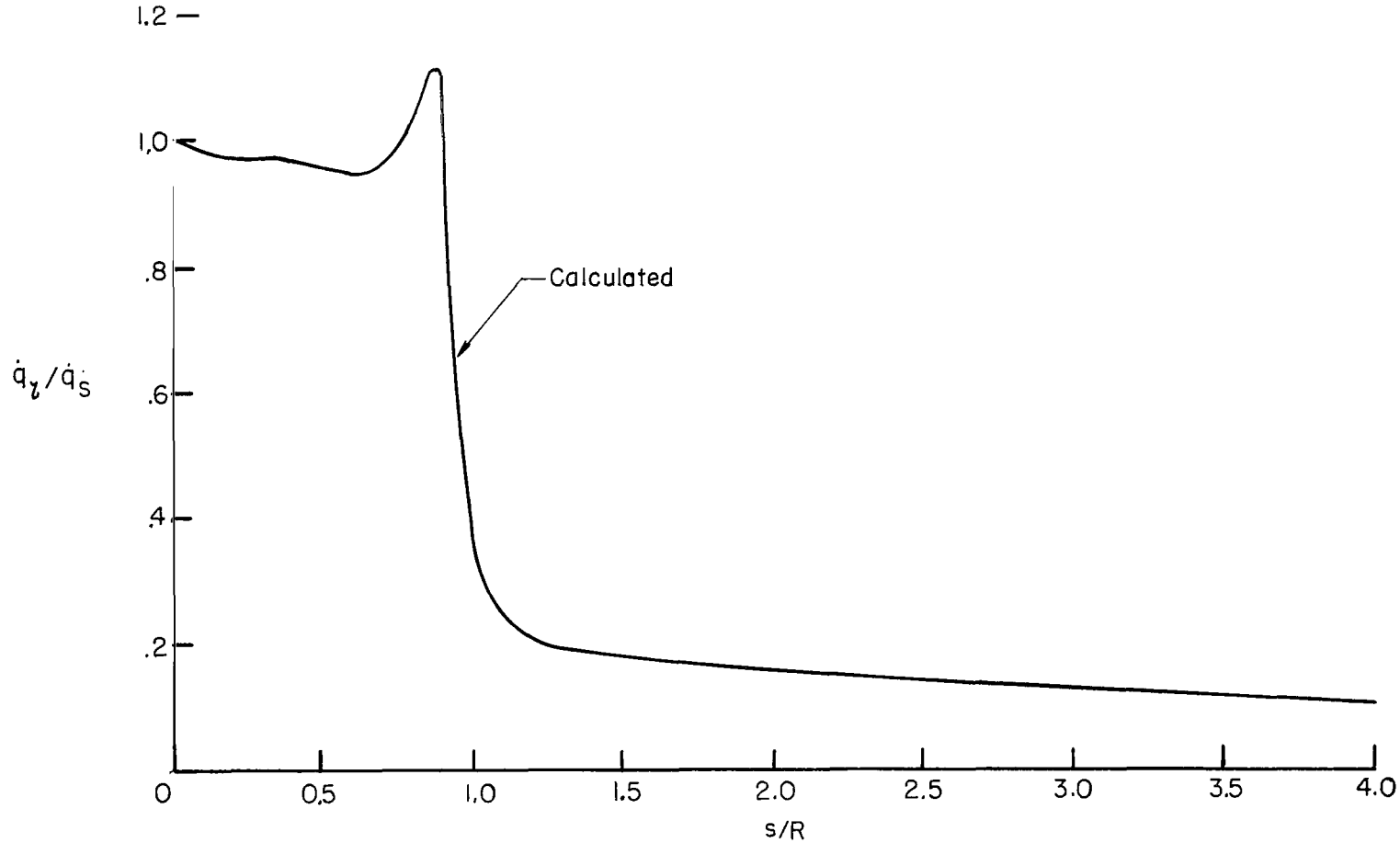


(b) $p_c$ = 232 psia; $p_{t,2}$ = 154 psia; $T_t$ = 4000° R ($p_c$ = 1.60 MN/m$^2$; $p_{t,2}$ = 1.06 MN/m$^2$; $T_t$ = 2220° K).

Figure 29.- Concluded.

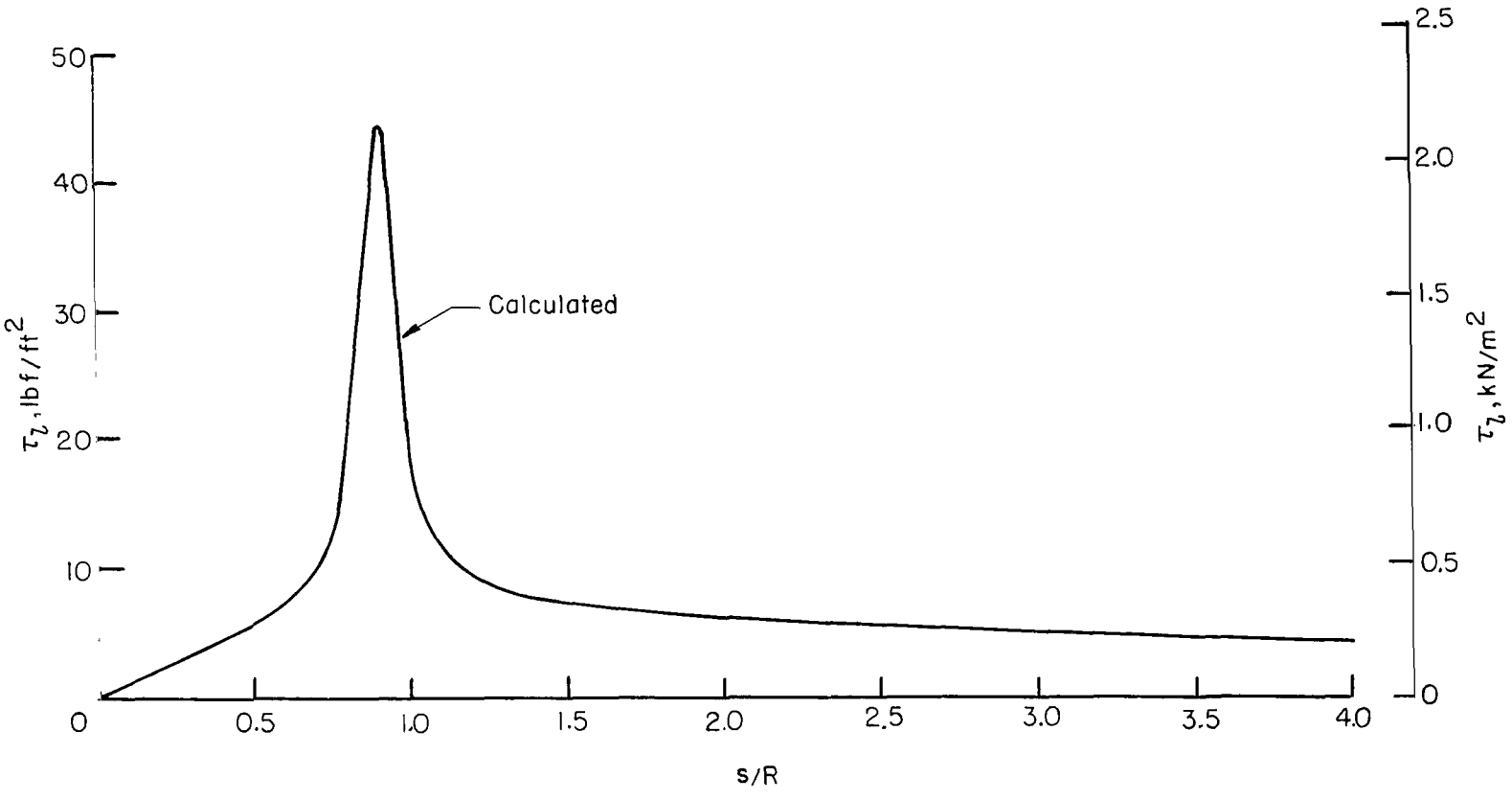


(a) $p_c$ = 121 psia; $p_{t,2}$ = 84 psia; $T_t$ = 2160° R ($p_c$ = 0.83 MN/m$^2$; $p_{t,2}$ = 0.56 MN/m$^2$; $T_t$ = 1200° K).

Figure 30.- Calculated aerodynamic shear distribution over blunt-nose cylinder model on 1-inch (2.5-cm) nozzle.

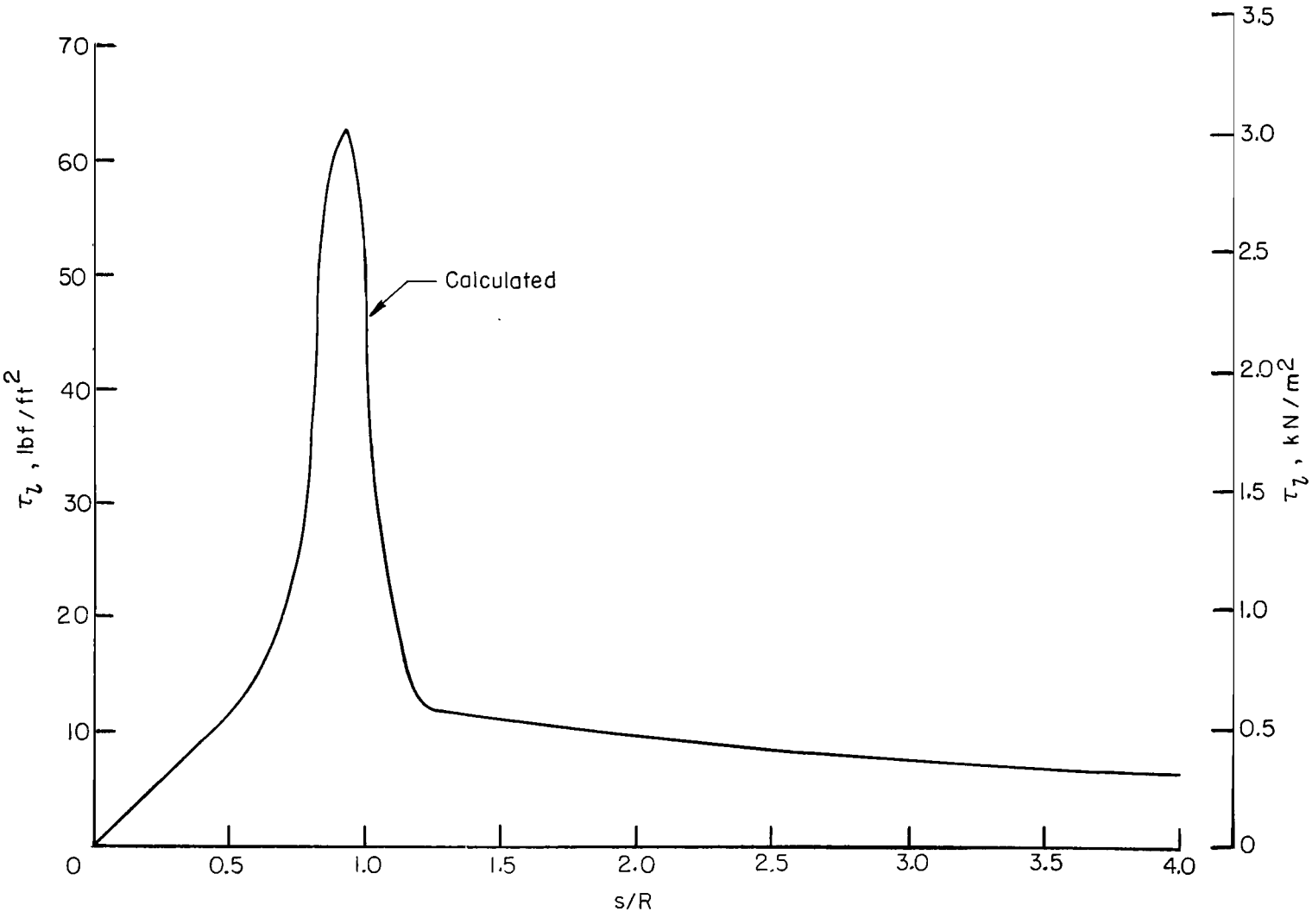


(b) $p_c$ = 232 psia; $p_{t,2}$ = 154 psia; $T_t$ = 4000° R ($p_c$ = 1.60 MN/m$^2$; $p_{t,2}$ = 1.06 MN/m$^2$; $T_t$ = 2220° K).

Figure 30.- Concluded.

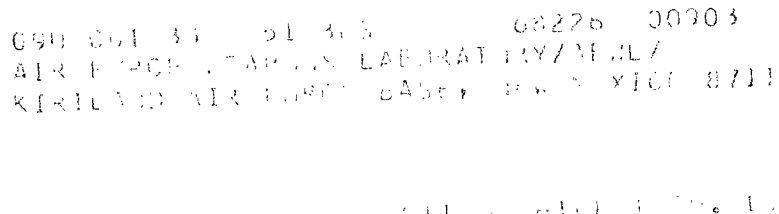



*"The aeronautical and space activities of the United States shall be conducted so as to contribute . . . to the expansion of human knowledge of phenomena in the atmosphere and space. The Administration shall provide for the widest practicable and appropriate dissemination of information concerning its activities and the results thereof."*

—NATIONAL AERONAUTICS AND SPACE ACT OF 1958

# NASA SCIENTIFIC AND TECHNICAL PUBLICATIONS

TECHNICAL REPORTS: Scientific and technical information considered important, complete, and a lasting contribution to existing knowledge.

TECHNICAL NOTES: Information less broad in scope but nevertheless of importance as a contribution to existing knowledge.

TECHNICAL MEMORANDUMS: Information receiving limited distribution because of preliminary data, security classification, or other reasons.

CONTRACTOR REPORTS: Scientific and technical information generated under a NASA contract or grant and considered an important contribution to existing knowledge.

TECHNICAL TRANSLATIONS: Information published in a foreign language considered to merit NASA distribution in English.

SPECIAL PUBLICATIONS: Information derived from or of value to NASA activities. Publications include conference proceedings, monographs, data compilations, handbooks, sourcebooks, and special bibliographies.

TECHNOLOGY UTILIZATION PUBLICATIONS: Information on technology used by NASA that may be of particular interest in commercial and other non-aerospace applications. Publications include Tech Briefs, Technology Utilization Reports and Notes, and Technology Surveys.

*Details on the availability of these publications may be obtained from:*

**SCIENTIFIC AND TECHNICAL INFORMATION DIVISION**

**NATIONAL AERONAUTICS AND SPACE ADMINISTRATION**

**Washington, D.C. 20546**